Rapid aqueous phase SO_2 oxidation during winter fog in the Indo-Gangetic Plain

Himanshu Sachan

A dissertation submitted for the partial fulfillment of BS-MS dual degree in Science

Indian Institute of Science Education and Research Mohali

April 2013

Certificate of Examination

This is to certify that the dissertation titled "**Rapid aqueous phase SO_2 oxidation during winter fog in the Indo-Gangetic Plain**" submitted by **Mr. Himanshu Sachan** (Reg. No. MS08024) for the partial fulfillment of BS-MS dual degree program of the Institute, has been examined by the thesis committee duly appointed by the Institute. The committee finds the work done by the candidate satisfactory and recommends that the report be accepted.

Dr. K. S. Viswanathan Dr. Vinayak Sinha Dr. Bärbel Sinha

(supervisor)

Dated: April 26, 2013

Declaration

The work presented in this dissertation has been carried out by me under the guidance of Dr. Bärbel Sinha at the Indian Institute of Science Education and Research, Mohali.

This work has not been submitted in art or in full for a degree, a diploma, or a fellowship to any other university or institute. Whenever contributions of others are involved, every effort is made to indicate this clearly, with due acknowledgement of collaborative research and discussions. This thesis is a bonafide record of original work done by me and all sources listed within have been detailed in bibliography.

Himanshu Sachan

(Candidate)

MS08024

April 26, 2013

In my capacity as the supervisor of the candidate's project work, I certify that the above statements by the candidate are true to the best of my knowledge.

Dr. Bärbel Sinha

(Supervisor)

Acknowledgement

I am grateful to my supervisor Dr. Bärbel Sinha and also Dr. Vinayak Sinha for their continuous support and insight which helped me in carrying out the project.

I would like to thank Dr. K. S. Viswanathan and Dr. Sanjay Mandal for the valuable discussions which helped in better understanding of the subject.

I would like to thank Dr. K. S. Viswanathan and Dr. Vinayak Sinha, the members of the examining committee for approving my thesis.

I would also like to thank my group members Mr. Vinod Kumar, Mr. Chinmoy Sarkar, Mr. Prafulla Chandra and Ms. Saryu Garg for their support and co-operation.

I thank the IISER Mohali Air quality facility for the data and infrastructure facilities. I thank Department of Science and Technology (DST) for the INSPIRE fellowship.

In the end I would also like to thank the IISER Mohali library and computer center for providing me the required literature for carrying out the project.

Mr. Himanshu Sachan

Contents

List of figures

List of tables

Abbreviations

IPCC: Intergovernmental Panel on Climate Change

sCIs: Stabilized Criegee Intermediates

VOC: Volatile Organic Compounds

TMIs: Transition Metal Ions

AAQS: Ambient Air Quality Station

IGP: Indo-Gangetic Plain

UV: Ultra Violet

PMT: Photo Multiplier Tube

ZAG: Zero Air Generator

MFCs: Mass flow Controllers

HG: Hygroscopic Growth

LWC: Liquid Water Content

Solar_rad: Solar radiation

RH: Relative Humidity

Abstract

This study provides a report on SO_2 measurements from IISER Mohali – Ambient Air Quality Station. We use strong point sources of SO_2 within the region with known SO_2/CO emission ratio for industries 50 km east of our measurement site respectively, to estimate the loss rate of SO_2 in wintertime fog in the Indo Gangetic Plain (IGP). The observed loss rate of SO_2 is faster than the maximum loss rate through oxidation by H_2O_2, OH and O_3 in the aqueous phase. Models including TMI and Criegee Intermediates may be able to explain the observed loss rates as the pollution plume studied originates from metal industries.

Chapter 1

Introduction

Sulfur dioxide is the most important anthropogenic sulfur containing air pollutant present in ambient atmosphere. SO_2 concentration ranges from the values as low as 20 pptV unpolluted marine background air to several hundred ppbV in plumes emitted from anthropogenic point sources. SO_2 is emitted directly from fossil fuel combustion, industries, biomass burning and volcanic eruptions, and produced in the atmosphere by the oxidation of reduced sulfur compounds like H_2S, carbonyl sulfide (OCS) and Dimethyl Sulfide (DMS), which is mostly emitted by phytoplankton present in oceans.

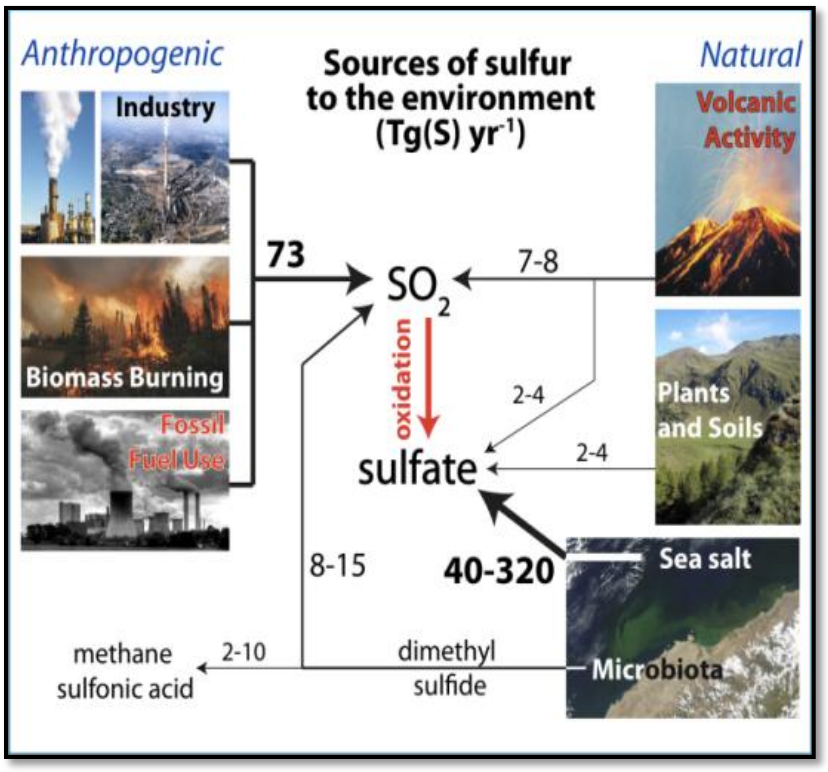

Figure 1.1: Various sources of sulfur and their source strength in the ambient atmosphere (Seinfeld and Pandis, Wiley and Sons, 1998).

The stratospheric sulfate layer (Junge Layer)(Junge, 1961), which has a strong impact on the Earth's radiative balance due to its ability to scatter incoming solar radiation, is maintained through photolysis and subsequent oxidation of OCS (Crutzen, 1976) in the troposphere. Sporadic injection of SO_2 into the stratosphere by Plinian volcanic eruptions leads to global cooling, which persists for 1-2 years (last observed after the Mt. Pinatubo eruption in 1991)(Pueschel, 1995).

Oxidation of SO_2 leads to the formation of sulfate particles which are the important components of atmospheric aerosols and cool the Earth's surface (Berresheim et al., 2002). Sulfate aerosols are present in the troposphere as well as the stratosphere.

Study of atmospheric SO_2, its lifetime and oxidation pathways is important because their oxidation pathways affect the size distribution and lifetime of the sulfate formed and, thereby, the total radiative energy budget of the Earth. Sulfate aerosol particles play an important role in the Earth's radiative balance through their direct and indirect effects. The aerosol direct radiative effect is the extinction/reflection of sunlight by the aerosols present in the sky. The indirect radiative effect of aerosol relates to the capability of aerosol particles to increase cloud brightness by reducing cloud droplet size (1^{st} indirect effect) and increase the lifetime of clouds by reducing the precipitation efficiency (2^{nd} indirect effect)(Solomon et al., 2007).

Sulfate particles are produced in the atmosphere by the oxidation of SO_2 that can take place in the gas phase and in the aqueous phase. It can also take place on the surface of mineral dust and sea salt aerosol.

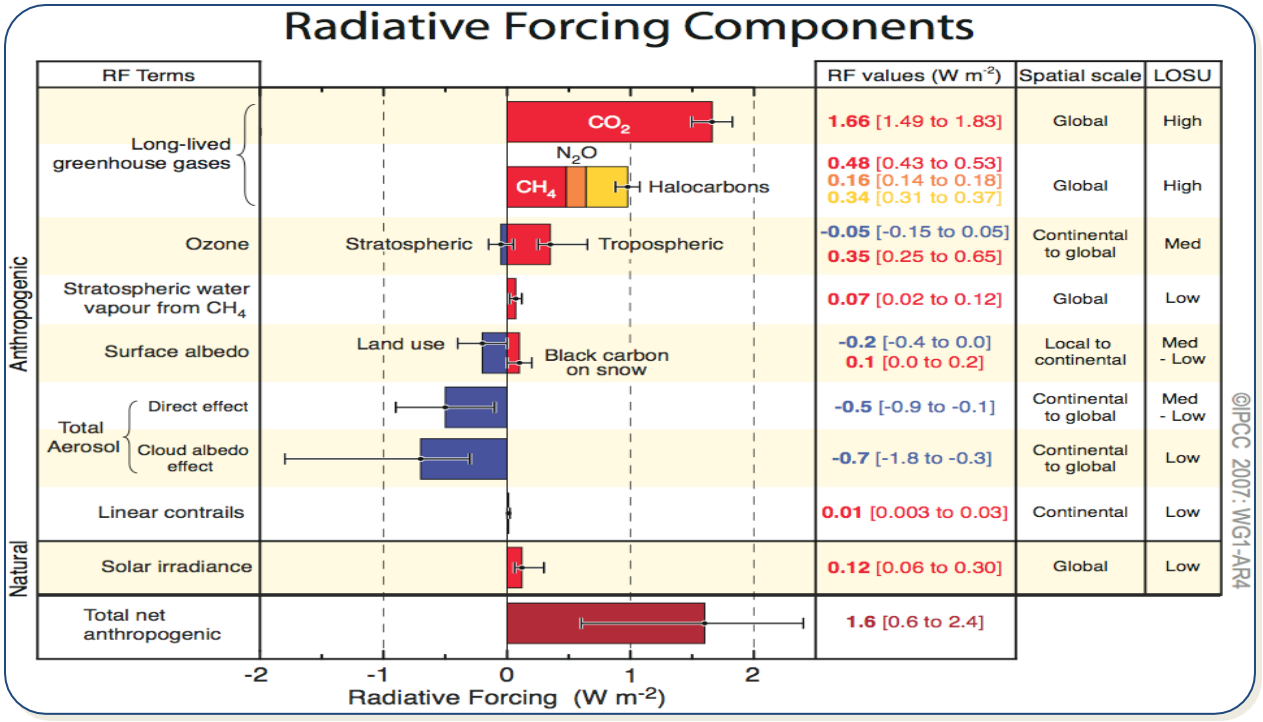

Figure 1.2: Radiative forcing: IPCC - Climate Change 2007 (Solomon et al., 2007).

1.1 Oxidation of SO_2 in the gas phase

Gas phase H_2SO_4 predominantly produced by oxidation of SO_2 by the OH is critical in controlling the formation of new particles into the atmosphere through nucleation (Benson at al., 2008; Berndt et al., 2008; Laaksonen et al., 2008; Kulmala, 2003; Kulmala et al., 2004). Gas phase oxidation of SO_2 is predominantly initiated by OH radicals (with atmospheric abundance of ≈ 0.1 pptV) that are formed in the atmosphere by the photolysis of ozone. Rate coefficients for reactions 1-3 were taken from Atkinson et al., 2004.

$$\mathbf{SO_2 + OH + M \xrightarrow{k1} HOSO_2 + M} \qquad (1)$$

At 298K,

$$k_01 = 4.5 \times 10^{-31} [N_2] \text{ cm}^3 \text{ molecule}^{-1} \text{ sec}^{-1}$$

$$k_\infty 1 = 1.3 \times 10^{-12} \text{ cm}^3 \text{ molecule}^{-1} \text{ sec}^{-1}$$

Where k_{01} and $k_{\infty 1}$ are rate coefficients for reaction (1).

The reaction is pressure dependent due to the need for the presence of a third collision partner.

The reaction has a temperature dependence over the range 200 – 300K for k_0 and k_∞ as shown below. Reaction (1) is followed by reaction (2).

$$k_01\,(T) = 4.5 \times 10^{-31}\,(T/300)^{-3.9}\,[N_2]\ cm^3\ molecule^{-1}\ sec^{-1}$$

$$k_\infty 1\,(T) = 1.3 \times 10^{-12}\,(T/300)^{-0.7}\ cm^3\ molecule^{-1}\ sec^{-1}$$

$$\mathbf{HOSO_2 + O_2 \xrightarrow{k2} HO_2 + SO_3} \qquad (2)$$

At 298K,

$$k2 = 4.3 \times 10^{-13}\ cm^3\ molecule^{-1}\ sec^{-1}$$

Where k2 is the rate coefficient for equation (2) and has a temperature dependence over the range 290-420 K.

$$k2\,(T) = 1.3\times10^{-12}\ e^{-330/T}\ cm^3\ molecule^{-1}\ sec^{-1}$$

Sulfur trioxide, in the presence of water vapor, is converted to sulfuric acid:

$$\mathbf{SO_3 + H_2O \xrightarrow{k3} H_2SO_4} \qquad (3)$$

$$k3 = 5.7\times10^4\ s^{-1} \text{ at } 50\% \text{ Relative Humidity}$$

Where k_3 is the rate coefficient for reaction (3).

The rate coefficient with other gas phase radicals such as the HO_2 radical $k_{298} < 1\times 10^{-18}\ cm^3\ molecule^{-1}\ sec^{-1}$, the NO_3 radical $k_{298} < 1\times 10^{-19}\ cm^3\ molecule^{-1}\ sec^{-1}$ and with $O(^3P)$ $k_0 = 1.4 \times 10^{-33}[N_2]\ cm^3\ molecule^{-1}\ sec^{-1}$ at 298K is much lower compared to the rate coefficient with OH. Therefore for a long time the reaction with OH was considered to be the only significant reaction producing H_2SO_4 (gas) in the troposphere. H_2SO_4 (gas) controls new particle formation in the continental and remote marine atmosphere. Nucleation results in a large number of particles that are small in size thus affecting the total particle number density (and hence aerosol scattering). Sulfate aerosol is also capable of hygroscopic growth at sub saturation relative humidity and is highly efficient as CCN thus it has a strong effect on atmospheric cloud albedo. The life time of SO_2 with respect to gas phase oxidation is about 10 days.

Recently a new gas phase oxidation process has been reported by Boy et al. (2012), which shows that oxidation of SO_2 by stabilized Criegee Intermediate radicals (sCIs) is crucial source for atmospheric sulfuric acid production in VOC rich environments. It was observed that the contribution of organic compounds though the reaction of sCIs to atmospheric sulfuric acid gas phase concentrations could be as high as 50% at ground level and is expected to be high where the concentrations of organic compounds are highest.

Ozonolysis of alkenes with addition of excess of ozone leads to formation of primary ozonide having high excess energy. This excess energy leads to the decomposition and thus forming Criegee Intermediate. The CIs formed still have excess energy and this excess energy is either released by decomposition or is stabilized to form sCIs.

$$\mathbf{Isoprene + O_3 \xrightarrow{k4_1} CH_2OOE \xrightarrow{k4_2} CH_2OO + SO_2 \xrightarrow{k4_3} SO_3 + H_2O} \quad (4)$$

$$k4_1 = 1.03 \times 10^{-14} \, e^{(-1995/T)} \times 0.3 \text{ cm}^3 \text{ s}^{-1}$$

$$k4_2 = 1 \times 10^6 \times 0.22 \text{ s}^{-1}$$

$$k4_3 = 3.9 \times 10^{-11} \text{ cm}^3 \text{ s}^{-1}$$

Global modeling studies followed the discovery and supported only weak sensitivity of the global direct and indirect aerosol forcing to this new source of OH (Pierce et al., 2013). However, the revised master chemical mechanism presented by Pierce et al. 2013 is not capable of reproducing measured aerosol size distributions in the Boreal forest and in the Amazon rain forest. Nucleation mode (< 10 nm) and Aitken mode (< 100 nm) number concentrations are crossly overestimated by the model. Aerosol number concentrations are overestimated by 50 -100 cm^{-3} throughout all sizes and >500-1500 cm^{-3} for nucleation mode particulate. The addition of the new gas phase oxidation process has only worsened the model-measurement gap in particular over the Amazon rain forest where the model predicts nucleation to occur in an environment in which nucleation has never been observed (Pöhlker at al., 2012). For the Amazon rain forest the model is also incapable of reproducing the observed Hoppel gap (Hoppel et al., 1994.) This is an indication that aqueous phase or multiphase reactions, capable of rapidly transferring gas-phase educts into accumulation mode (>100 nm) particulate matter while bypassing the nucleation resulting in

condensational growth scheme implemented in global models are missing in the model. The overestimation across all size ranges and the fact that the overestimation for the rainy season in the Amazon rain forest is worse than the overestimation for the boreal forest points towards an underestimation of wet deposition by the model.

1.2 Oxidation of SO_2 in the aqueous phase

A large number of potential oxidants can participate in aqueous phase oxidation of SO_2, though O_3, H_2O_2 and transition metal ion catalyzed oxidation by O_2 are considered to be the only three pathways relevant on a global scale. All these 3 oxidants are produced photo-chemically in the atmosphere in the gas phase.

Reaction starts with the dissolution of SO_2,

$$\mathbf{SO_2\,(g)} \overset{k5}{\leftrightarrow} \mathbf{SO_2.H_2O} \tag{5}$$

$$k5 = 1.23 \times e^{(3020 \times T_{fac})}\ \text{M/atm (Henry Law Constant)}$$

Where M = Molarity (mol L^{-1})

Followed by dissociation of $SO_2.H_2O$ to HSO_3^- and SO_3^{2-}

$$\mathbf{SO_2.H_2O} \overset{k6}{\leftrightarrow} \mathbf{HSO_3^-(aq.) + H^+(aq.)\ (pK_a = 1.9)}\ \text{(Eriksen, 1972)} \tag{6}$$

$$k6 = 1.23 \times 10^{-2} \times e^{(2010 \times T_{fac})}\ \text{M}$$

$$\mathbf{HSO_3^-\,(aq.)} \overset{k7}{\leftrightarrow} \mathbf{SO_3^{2-}(aq.) + H^+(aq.)\ (pK_a = 7.2)} \tag{7}$$

(Moore, Stanitski and Jurs, Brools/Cole – Thomson Learning, USA, 2005)

$$k7 = 6.0 \times 10^{-8} \times e^{(1120 \times T_{fac})}\ \text{M}$$

Reaction with O_3,

$$\mathbf{O_3\,(aq.) + SO_3^{2-}(aq.)} \overset{k8}{\leftrightarrow} \mathbf{SO_4^{2-}(aq.) + O_2\,(aq.)} \tag{8}$$

$$k8 = 1.8 \times 10^{4} \times [H^+]^{-0.4}\ \text{M s}^{-1}$$

Reaction with H_2O_2,

$$\mathbf{H_2O_2\,(aq.) + HSO_3^-(aq.) \overset{k9}{\leftrightarrow} H^+\,(aq.) + SO_4^{2-}(aq.) + H_2O} \quad (9)$$

$$k9 = (8.0 \times 10^4 \times e^{(-3650 \times T_{fac})})/(0.1 + [H^+])\ M\ s^{-1}$$

Rate coefficients for reactions 5 to 7 were taken from Seinfeld and Pandis, 1998; Berglen et al. 2004). Rate coefficients for reactions 8 and 9 were taken from Berglen et al. 2004. However, to accurately calculate the loss rate due to this reaction at a specific pH it is insufficient to assume that the oxidant is always available in the aqueous phase in excess. Instead the uptake of the oxidant from the gas phase into the aqueous phase needs to be explicitly considered. Competing reactions of the oxidant in the aqueous phase also need to be considered if the competing reaction has a faster rate coefficient than the reaction with SO_3^{2-}. Rate coefficients for reactions 10 and 11 were taken from Berglen et al. 2004.

$$\mathbf{O_3\,(g) \overset{k10}{\leftrightarrow} O_3\,(aq.)} \quad (10)$$

$$k10 = 1.13 \times 10^{-2} \times e^{(2300 \times T_{fac})}\ M/atm\ (Henry\ Law\ Constant)$$

$$\mathbf{H_2O_2\,(g) \overset{k11}{\leftrightarrow} H_2O_2\,(aq.)} \quad (11)$$

$$k11 = 7.1 \times 10^4 \times e^{(6800 \times T_{fac})}\ M/atm\ (Henry\ Law\ Constant)$$

Where $T_{fac} = 1/T - 1/298.15$ (Berglen et al., 2004).

The rate of reaction 8 is significant only at pH > 6. H_2O_2 is the dominant oxidant under typical bulk cloud pH conditions (pH < 5) (Alexander et al., 2005).

In the polluted urban atmosphere and plumes from point sources NO_2, NO_3 (Feingold et al., 2002) and HNO_4 (Dentener et al., 2002) are considered to be of local importance. Rate constants of the reaction of S(IV) oxide species with NO_2, NO_3 radical and HNO_4 are $1.54 \times 10^7\ M^{-1}\ s^{-1}$ at pH 6.7, $1.4 \times 10^9\ M^{-1}\ s^{-1}$ at pH 4.5 and $1.9 \times 10^5\ M^{-1}\ s^{-1}$ for pH 2-4 respectively. (Brant and Eldik et al. 1995).

The solubility of SO_2 in dependent on pH and decrease with decreasing pH. Different SO_2 species are dominant at different pH for ex. $SO_2.H_2O$ at < 1.5 pH, HSO_3^- (hydrogen sulfite

anion) at pH 1.5 – 6 and SO_3^{2-} (sulfite anion) at pH > 6. So depending on pH HSO_3^- and SO_3^{2-} species are the major sulfur species present in atmospheric water droplet, so these two species along with $SO_2.H_2O$ are regarded as the total dissolved S (IV).

Oxidation of SO_2 by O_2 catalyzed by transition metal ions (TMIs) been known for many years now and the kinetics of the reaction have been studied mostly for Fe (III) and Mn (II) (Zuo and Zhan, 2005; Tursic et al., 2003; Kotronarou and Sigg, 1993; Martin and Hill, 1987).

Below is a chain mechanism of iron-oxygen-S (IV) system proposed by Deguillaume et al. 2005.

$$\mathbf{Fe\ (III) + HSO_3^- \rightarrow Fe\ (II) + SO_3^- + H^+} \quad (12)$$

$$\mathbf{SO_3^- + O_2 \rightarrow SO_5^-} \quad (13)$$

$$\mathbf{SO_5^- + Fe\ (II) + H^+ \rightarrow HSO_5^- + Fe\ (III)} \quad (14)$$

$$\mathbf{HSO_5^- + Fe\ (II) \rightarrow SO_4^- + OH^- + Fe\ (III)} \quad (15)$$

$$\mathbf{SO_4^- + Fe\ (II) \rightarrow SO_4^{2-} + Fe\ (III)} \quad (16)$$

Fe, Ti, Mn, Cr and Ni were found to be leached in significant quantities from Sahara dust (descending order of abundance), while Zn, Fe^{3+}, Ni, Cu, Fe^{2+} and Mn (descending order of abundance) were found in cloud water at a remote continental site in Europe. Out of this list the synergistic effect of only two transition metals, namely Fe and Mn have been studied in detail[15] and increases the SO_2 oxidation rate by ten folds compared to reaction with individual metal ions. One study found that in the presence of Fe (III), Mn (II) and Pb (II) the reaction rate is further enhanced (Graedel and Weschler, 1981; Grgic et al., 1991). Copper, cobalt (Bengtsson and Bjerle, 1975) and nickel were found to be less efficient in catalyzing S (IV) oxidation, Zn was not found to be catalytically active and Vn (V) inhibits S (IV) oxidation by Fe(III) (Brandt and Elding, 1998). The catalytic activity of Cr depends on its speciation. Cr (III) but forms a Chromium (III)-sulfito complex but is not catalytically active in S (VI) oxidation while Cr (VI) is catalytically active and shows a drastic decrease of reaction rate with increasing pH. The relative humidity and total water content in aerosols play important role in the catalytic activity of TMI as mineral dust, an important source of

TMI is hydrophobic and the total amount of mineral dust particles found in fog/cloud droplets increases with increasing supersaturation.

The sulfate particles formed by aqueous phase oxidation are bigger in size compared to gas phase oxidation and do not lead to the nucleation of new particles. Aqueous phase oxidation is thought to occur in clouds and fog though global climate chemistry models consider only the in-cloud oxidation explicitly.

Aerosols found in atmosphere can be classified into 3 types, Aitken mode particles (<100 nm), accumulation mode particles (0.1 - 2.5 μm) and coarse particles (2.5-100 μm) (Brandt and Eldik, 1995). Fine particles mostly contain acidic anions like SO_4^{2-}, NO_3^- and $C1^-$, balanced by NH_4^+, Na^+, Ca^{2+} and K^+. Fine aerosol can be secondary in nature, i.e. produced by reactions from gas phase compounds, though several types of primary aerosol particles are also found in the "fine" size range (soot, mineral dust, primary, organic aerosol (POA) and primary biogenic particles). The coarse particles are mostly primary in nature and are directly emitted from deserts (mineral dust), sea spray (sea salt), the biosphere (pollen, fungal spores, fragments of other biogenic material) and anthropogenic activity (e.g. fly ash, road dust, tire wear, dust from construction activity). Aerosols can contain both soluble particles like salts and insoluble particles like metal oxides. These soluble aerosols particles are particularly efficient as cloud condensation nuclei as they reduce the super-saturation required for condensation of water droplets.

In this thesis we have estimated and reported the loss rate of SO_2 emitted from regional sources during the winter fog, in the Indo-Gangetic plain, and have compared the loss rates with a box modeling study performed for pH ~ 7 (Venkataraman et al., 2006) which considers several reactions that are neglected in global climate chemistry models, which generally prescribe a cloud pH of 4-5 and, therefore, reduce the chemistry to a subset of reactions relevant in this pH range with already present models. We have used a source-receptor model to locate a suitable point source to investigate the sulfate chemistry in the Indo-Gangetic plain. We estimate SO_2 loss rates and sulfate production rates under a variety of relative humidities which result in different aerosol liquid water availability.

Chapter 2

Material and Methods

2.1 Site description

We report measurements of SO_2 measurements from IISER Mohali – Ambient Air Quality Station (30.67°N, 76.73°E), a station located at a suburban site in the Indo Gangetic Basin (IGB) during wintertime (10th Dec. 2011 to 29th Feb. 2012). The research site at Mohali is located in the northern part of India, in the state of Punjab. The height of Mohali is 310 meters above mean sea level. As the site is far away from the moderating influence of sea, it experiences a continental climate.

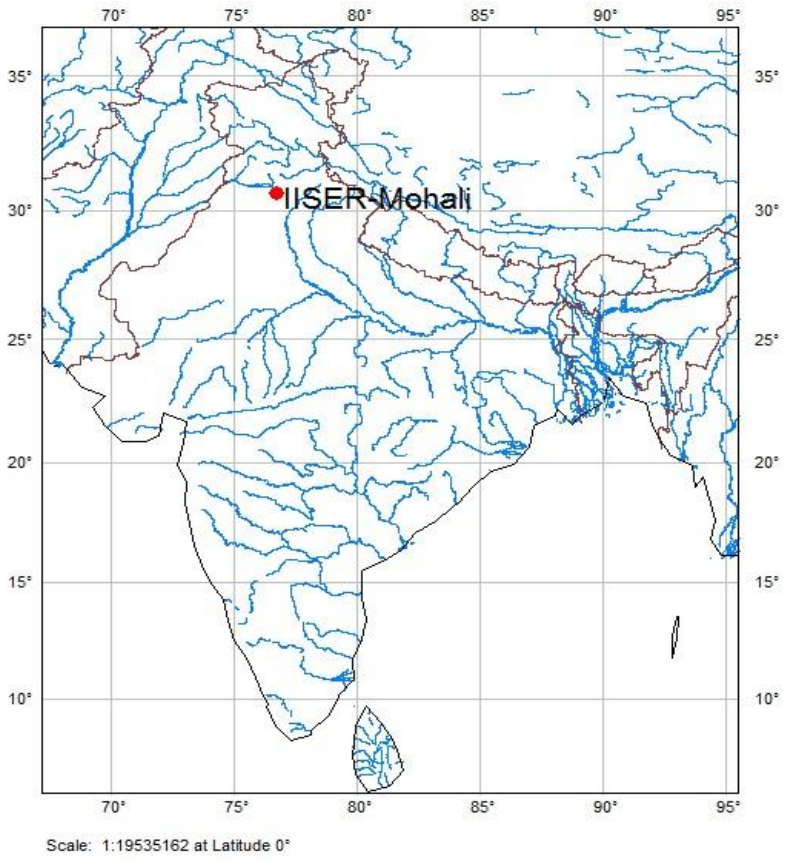

Figure 2.1: Location of the receptor site, IISER Mohali.

The climate in Mohali is divided into 4 main seasons, summer (March - June), monsoon (July – mid of September), post monsoon (mid of September - November) and winter (December - February) based on the variation in temperature, rainfall, relative humidity and solar radiation. The end of monsoon and start of the post-monsoon season is marked by the last monsoon rainfall. The beginning of winter is marked by nigh-time temperatures dropping to values < 5°C and the occurrence of wintertime fog. The end of the winter season and beginning of summer (pre-monsoon) season is marked by a rise in nighttime temperatures and a drop in RH associated with rising daytime temperature. This transition also marks the end of wintertime fog events. The first monsoon showers and a ~ 3°C drop in temperatures mark the onset of the next monsoon season. However, the data that is recorded by IISER Mohali Air Quality Station shows that there is relatively high emission of Carbon Monoxide (CO), NOx and volatile organic compounds from the end of October through-out November which is due to intensive bio-mass (crops) burning during this period. Therefore we divided the post monsoon into clean and polluted post monsoon.

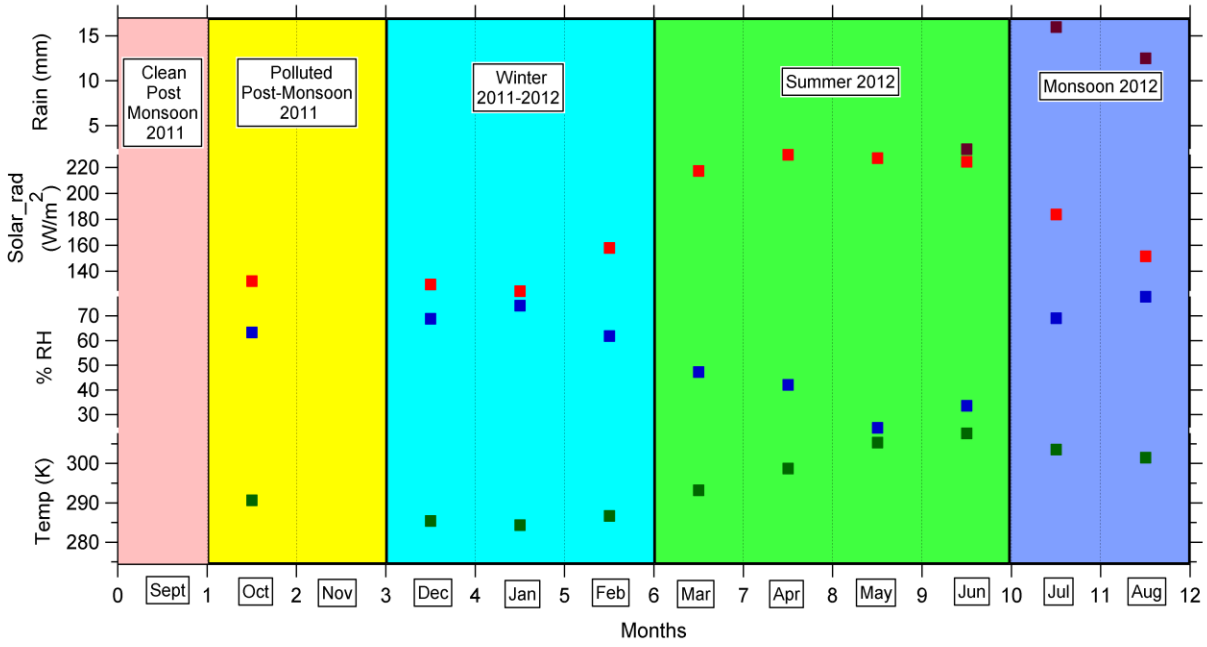

Figure 2.2: Monthly Averages for temperature, %RH, solar radiation and rainfall at IISER Mohali from September 2011 to August 2012.

2.2 Measurement of SO_2 at IISER Mohali Air Quality Station

2.2.1 Instrumentation

SO_2 has 3 regions of absorption in UV region. First is weak absorption in 390-340 nm, second and stronger absorption in the region 320-250 nm and third and several times stronger absorption in the 230-190 nm region.

The absorption region between 230-190 nm has an estimated lifetime of 9×10^{-9} sec (Okabe, 1971) which can be attributed to predissociation. Ambient air shows no quenching effect on fluorescence produced by Zn 213.8 nm line. On the other hand, fluorescence produced by absorption in the region 320-250 nm is strongly quenched by air. Therefore, the absorption line at 213 nm is used for measurement of ambient SO_2 concentrations.

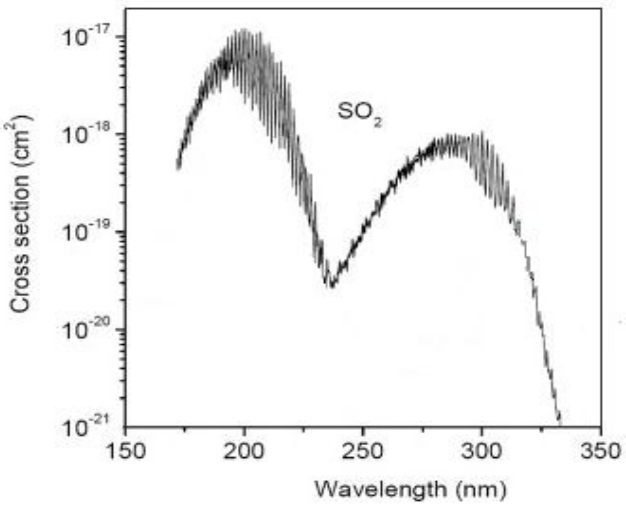

Figure 2.3: Cross-section of molecular absorption of SO_2 in the UV region. (Modified – Lyons, 2008).

Sulfur dioxide has a stronger absorption in emission lines of 218.9nm and 220.8nm (Zhenjiang et al., 2002). The exciting wavelength should coincide with the absorption peaks to give the maximum fluorescence intensity. There are 3 options for light source that lie within the required region namely Zn lamp (213.8 nm), Sb lamp (217.5 nm) and the Cd lamp

(227.8 nm). It was observed through experiments that atmospheric air shows almost no quenching effect on the fluorescence produced by the Zn 213.8 nm line, so Zn lamp is used. The signal of SO_2 fluorescence is very weak, thus PMT was used as a detector in the monitor system.

2.2.2 Working Principle

Measurement of ambient sulfur dioxide (SO_2) is based on the principles of fluorescence spectroscopy. SO_2 molecule absorbs ultraviolet (UV) light and gets excited at one wavelength and then decays to lower energy levels emitting UV light at some other wavelength.

SO_2 has a strong UV absorption at wavelength between 190 and 230 nm. The absorption of photons at these wavelengths results in emission of fluorescence photons at a higher wavelength (320-380 nm). By exciting SO_2 at 213.8 nm (absorption maxima) and measuring the intensity of fluorescence at 350 nm (emission maxima), SO_2 concentrations can be measured. The amount of fluorescence emitted is directly proportional to SO_2 concentration.

$$SO_2 + h\nu_1 \rightarrow SO_2^* \rightarrow SO_2 + h\nu_2$$

Where: $h\nu_1$ = incidence light

$h\nu_2$ = fluoresced light

SO_2^* = SO_2 in its excited state

All the SO_2 measurements at IISER Mohali are done using a pulsed fluorescence SO_2 analyzer (Model 43i, Thermo Fischer Scientific). The sample is flown into the analyzer thought a sample bulkhead after which it is passed through a hydrocarbon kicker which removes hydrocarbons from the sample by forcing the hydrocarbon molecules to permeate through the tube wall. It operates on a selective permeation principle using differential pressure to force hydrocarbon molecules to pass through the tube wall. The driving force for the hydrocarbon removal is the differential partial pressure across the wall. This differential pressure is produced within the instrument by passing the sample gas through a capillary tube

to reduce its pressure. The sample gas is then fed to the shell side of the hydrocarbon kicker. Condensing lens focuses the pulsating

UV light into the mirror assembly which reflects only the wavelengths that excite SO_2 molecules. A set of eight mirrors selectively reflects only those wavelengths used in exciting SO_2 molecules. This reflective filtering causes the radiation reaching the detection chamber to be more intense and more stable throughout the lifetime of the instrument. This radiation is then focused in the fluorescence chamber. The sample is passed through this camber and SO_2 is excited as shown in Figure 3. After the SO_2 molecules decay to lower energy state they emit UV light which is proportional to SO_2 concentration. The PMT is located at 90° from the UV lamp source on the axial center line of the reaction cell. The band-pass filter allows only the wavelength emitted by excited SO_2 molecules to reach the photomultiplier tube (PMT) mainly 320 – 380 nm, which detects the UV light emitted from excited SO_2 molecules. The emitted UV light intensity is proportional to concentration of SO_2. Sample after leaving the optical chamber is passed through a flow sensor, a capillary and the shell side of hydrocarbon kicker and is further flowed to the pump and is finally exhausted out. The internal pump and heaters all operate on 110V AC.

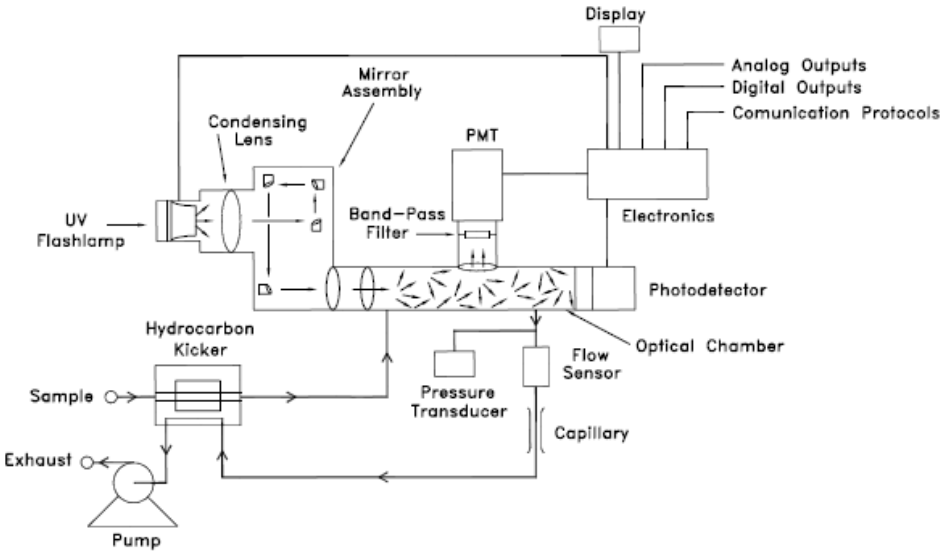

Figure 2.4: Flow Schematic of Pulsed Fluorescence analyzer (Pulsed Fluorescence Analyzer, 2008).

2.2.3 General problems with ambient SO_2 measurements

Water vapor may quench the fluorescence of SO_2 at certain wavelengths. The SO_2 signal decreases linearly with the percent increase of water in air. The presence of 2% H_2O reduces the signal by 25%. To counter this problem, proper selection of UV absorption wavelength is done.

For measurement of low concentration of SO_2, excitation by pulsed UV light is more useful as excitation is more efficient by a pulsed source as compared to a continuous source since pulsed source is a high intensity source of excitation with a low background (Omenetto and Boutilier, 1977). Pulsed mode improves the signal to noise ratio and has lower power requirements compared to continuous (< 1 Watt) (Pulsed Fluorescence Analyzer, 2008).

Polycyclic aromatic hydrocarbons (PAH) such as naphthalene (Atmospheric concentration ~ 0.2 ppb) exhibit strong fluorescence within the range of 300 - 400 nm with maxima between 320 - 350 nm which is within the spectral range of SO_2 and thus are a major interference. Xylene is another hydrocarbon that causes interference. This problem is countered using hydrocarbon kicker within the instrument that filters hydrocarbons out of the ambient air.

Nitric oxide (NO) fluoresces in a range close to that of SO_2. However Okabe et al. 2012 provides information that 500 ppb NO gives equivalent response of 1 ppb SO_2 (Okabe, 1971). NO values at IISER Mohali do not go beyond 146 ppb so the maximum uncertainty in SO_2 values due to NO is about 0.3 ppb, which is well within the uncertainty of SO_2 measurements. So the interference due to NO can be neglected.

2.2.4 Calibration and handling of SO_2 analyzer

Regular diagnostic check on daily basis is done to ensure proper functioning of analyzer, which includes checking of instrument parameters like internal temp., chamber temp., pressure, intensity of lamp and sample flow.

Table 2.1: Showing an example of the diagnostic check of SO_2 analyzer for 30th September 2012.

Date	Time	Inlet temp. (°C)	Chamber temp. (°C)	Pressure (mm Hg)	Flow (L/min)	Lamp intensity (%)
30-09-2012	15:35	30.9	45.3	767.8	0.374	92

Zero and Span calibration: Regular Zero and Span calibrations are must to ascertain the accuracy and reliability of the air quality data collected. A weekly zero drift is done where zero air (SO_2 free) is generated by Zero air generator (ZAG) and is passed though SO_2 analyzer and the recorded drift is set in the instrument for background values correction.

Span calibration is done monthly with 10, 20 30, 40 and 50 ppbV SO_2 concentrations and a calibration plot is generated between the inserted and observed SO_2 concentration. This plot provides the calibration background coefficient which is set in the instrument again for background correction and to make sure that the data that is being generated by the instrument has minimal instrumentation errors.

The detection limit achieved using this analyzer is 1ppb for 60 seconds averaging time.
Below are 2 tables showing overall zero-drift calibrations and span calibrations data done for SO_2 analyzer.

Table 2.2: Span calibrations with date and uncertainty of slope done at IISER Mohali for SO_2 analyzer.

Date	Slope	Uncertainty of slope	Intercept	Uncertainty of intercept
30/08/2011	0.936	-	-	-
09/11/2011	1.09	± 0.03	1.3	± 0.9
23/11/2011	0.986	-	-	-
03/01/2012	1.16	± 0.01	-1.9	± 0.3
28/02/2012	1.138	± 0.001	1.65	± 0.02
21/04/2012	0.99	± 0.05	0.2	± 0.9
22/06/2012	1.144	± 0.003	-1.94	± 0.07
25/09/2012	1.295	± 0.009	1.2	± 0.3
02/11/2012	1.038	± 0.005	-1.5	± 0.2
05/12/2012	1.10	± 0.05	-1.52	± 1.09
06/01/2013	0.87	± 0.01	-0.1	± 0.5
28/02/2013	0.86	± 0.002	-0.3	± 0.8

(Note: Calibrations on 30/08/2011 and 23/11/2011 were done by the instrument engineer so the uncertainty and intercept values are not provided.)

Table 2.3: Zero-drift calibrations with dates done at IISER Mohali for SO_2 analyzer.

Date	Zero Drift (ppb)	Date	Zero Drift (ppb)
30/08/2011	-0.019	21/04/2012	-0.02
22/09/2011	1.91	04/04/2012	0.05
26/09/2011	0.15	21/04/2012	-0.02
27/09/2011	0.01	08/05/2012	0.03
28/09/2011	0.01	24/05/2012	-0.03
29/09/2011	0.02	01/06/2012	0.01
30/09/2011	0.01	08/06/2012	-0.05
04/10/2011	0.01	18/06/2012	0.04

07/10/2011	0.03	22/06/2012	0.04
10/10/2011	0.01	18/07/2012	0.1
14/10/2011	0.01	20/07/2012	0.02
18/10/2011	0.15	03/08/2012	0.02
27/10/2011	0.02	28/08/2012	0.02
04/11/2011	0.02	03/09/2012	-0.09
09/11/2011	0.01	15/10/2012	0.03
03/01/2011	0.02	20/11/2012	0.02
16/01/2012	0.06	05/12/2012	-0.07
23/01/2012	0.05	13/12/2012	-0.01
30/01/2012	0.01	20/12/2012	-0.05
06/02/2012	0.01	29/12/2012	0.01
13/02/2012	0.02	14/01/2013	0.02
28/02/2012	0.03	30/01/2013	-0.04
12/03/2012	0.02	18/02/2013	-0.04
04/04/2012	0.05	28/2/2013	0.06

2.2.5 Uncertainty calculations

The data has an accuracy error due to uncertainty in the SO_2 gas cylinder which is 5% and uncertainty in 2 of the Mass Flow Controllers (MFCs) 2% each.
So percentage accuracy error is = 5.744%

Data has an additional accuracy error that comes out due to the drift in slope of the instrument in between two span calibrations and the zero drift. Percentage change in the slope between 2 consecutive calibrations provides the percentage uncertainty which is additional accuracy error.

The precision error can be observed by looking at 10-30 minutes of measurements while a set concentration of SO_2 is introduced into the instrument. The precision error can be estimated

by calculating the standard deviation of measurements when a constant concentration is introduced into the instrument.

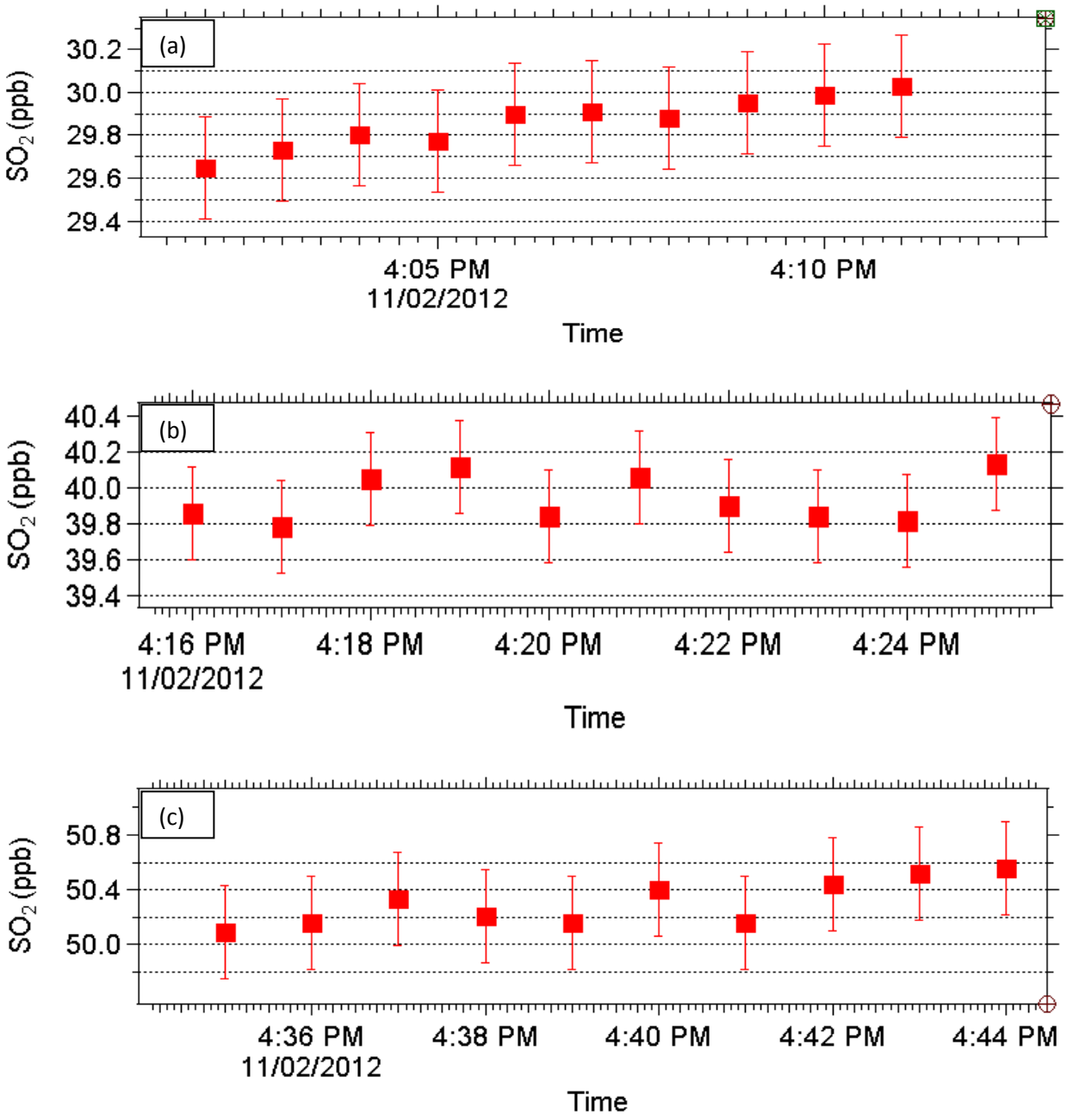

Figure 2.5: Precision measurement plots for (a) 30 ppb, (b) 40 ppb and (c) 50 ppb for a calibration on 11th February 2012.

Table 2.4: Provides the precision error in ppb and percentage uncertainty for 3 different concentrations introduced i.e. 30 ppb, 40 ppb and 50 ppb.

Introduced (ppb)	Precision error (ppb)	% error
30	0.12	0.4
40	0.13	0.3
50	0.17	0.3

Total = $\sqrt{\text{Precision error}^2 + \text{Accuracy error}^2}$

Uncertainty due to zero drift of the instrument is directly added to the total uncertainty.

So, Overall uncertainty = Total uncertainty + Zero drift of the instrument.

2.3 Source-receptor model

Residence-time weighted concentration back trajectory analysis is one of the most important techniques for identification of potential sources of a substance in a defined geographical area. This source-receptor model was generated in our lab (Garg, abstract, 2013) and is capable of identifying local and regional sources of air pollutants like Particulate Matter (PM), NOx, SO_2, VOCs. The model code assumes all the atmospheric transport to be Lagrangian and linearly extrapolates air masses reaching the receptor location, backwards in time for a fixed number of steps. For long lived species the model run is limited to < 3 hours as spatial uncertainty increases the longer an air-mass is linearly extrapolated back in time. Since the model is restricted to work/run only up to the corresponding lifetime of species, it is possible to estimate the local sources with confidence.

Using the model it was possible to identify the major sources of SO_2 for the region around IISER Mohali. Using the model, residence time weighted average concentration plots were generated for SO_2 for different time scales and were overlaid on Google Earth to find out the exact location of the possible sources.

2.4 Emission ratio

Emission ratios relate the emission of a particular species of interest to that of a reference species such as CO_2 or CO. Emission ratios are obtained by dividing the excess trace species concentrations measured in a fire plume by the excess concentration of a simultaneously measured reference gas. To obtain "excess" concentrations, the ambient background concentrations are subtracted from the values measures in the smoke (Andreae and Merlet, 2001).

SO_2 is produced in the atmosphere by the oxidation of reduced sulfur compounds like H_2S, carbonyl sulfide (OCS) and Dimethyl Sulfide (DMS), which is mostly emitted by phytoplankton present in oceans. SO_2 is also emitted directly from fossil fuel combustion and volcanic eruptions. Anthropogenic emissions are responsible for largest fraction for global SO_2 burden (Figure 1.1). The main source of sulfur dioxide is industrial activity, namely the combustion of sulfur containing fuel, for example coal, oil, bio-mass or gas that contains sulfur. Some mineral ores also contain sulfur, and sulfur dioxide is released when they are processed. SO_2 is also emitted from motor vehicle emissions, depending upon the sulfur content in the fuel.

Emission ratio is a term used for calculation of ratio between the species that are emitted from the same source. For example, combustion of coal or oil or any fuel leads to emission of both SO_2 and Carbon monoxide (CO). Some fuels emit higher concentration of one species compared to other species and thus we have variable emission ratios. CO has a chemical lifetime of around 1–2 months and can be transported over large distances, but intense local emission sources dominate the concentrations in the lowermost troposphere (Worden et al., 2012). CO is a by-product of combustion reactions and is emitted due to incomplete combustion of fuel. Motorized vehicles, industries using coal, domestic usage of coal and biofuels are the major sources of CO (Ohara et al., 2007). The SO_2/CO emission ratio is, therefore, a function of both, the sulfur content of the fuel and the efficiency of the combustion process.

Table 2.5: Regional emissions by emission sectors and fuel type (Modified)

Emissions	Fuel type	SO_2	CO	SO_2/CO
Domestic (Ohara et al., 2007)	Coal	165	2253	0.073
	Biofuel	348	56068	0.006
Transport (Ohara et al., 2007)	Oil	199	7093	0.028
Industries (Ohara et al., 2007)	Coal	490	4088	0.120
Power plants (Ohara et al., 2007)	Coal	2865	936	3.061
Biomass burning (Venkataraman et al., 2006)	Forest burning	0.04	5	0.008
	Agricultural waste	0.150	50	0.003

(Data is in Tg/year)

Table 1 shows overall SO_2 and CO emissions from various sources within India. As per the data given in the table it can be seen that the SO_2/CO emission ratio varies with the type of fuel. We also see that in general the observed SO_2/CO emission ratio at Mohali is at the lower end of the emission ratio from known sources (<0.016). Given the fact that several known sources for which a higher emission factor are expected to contribute significantly to SO_2 & CO mixing ratios observed at the station but are located upwind of the receptor site the observed SO_2/CO ratios seem to be at least partially controlled by SO_2 loss process. Sources around Mohali include:

- Traffic in particular from Chandigarh, Panchkula and Mohali (SO_2/CO emission ratio = 0.028)
- The 1000 MW coal fired power plant located near Rupnagar 45 km North of Mohali (SO_2/CO emission ratio = 3.061)

- Numerous industries in the Industrial areas of Chandigarh and Mohali and around Zirakpur, Dera Bassi and Kala Amb (SO_2/CO emission ratio = 0.12)
- Numerous brick kilns which operate throughout the year except during Monsoon season
- Regional crop residue burning during polluted post monsoon season and part of summer
  (SO_2/CO emission ratio = 0.003)
- Domestic combustion of biomass for cooking (throughout the year SO_2/CO emission ratio = 0.006) and heating (during winter).

2.5 Estimation of liquid water content

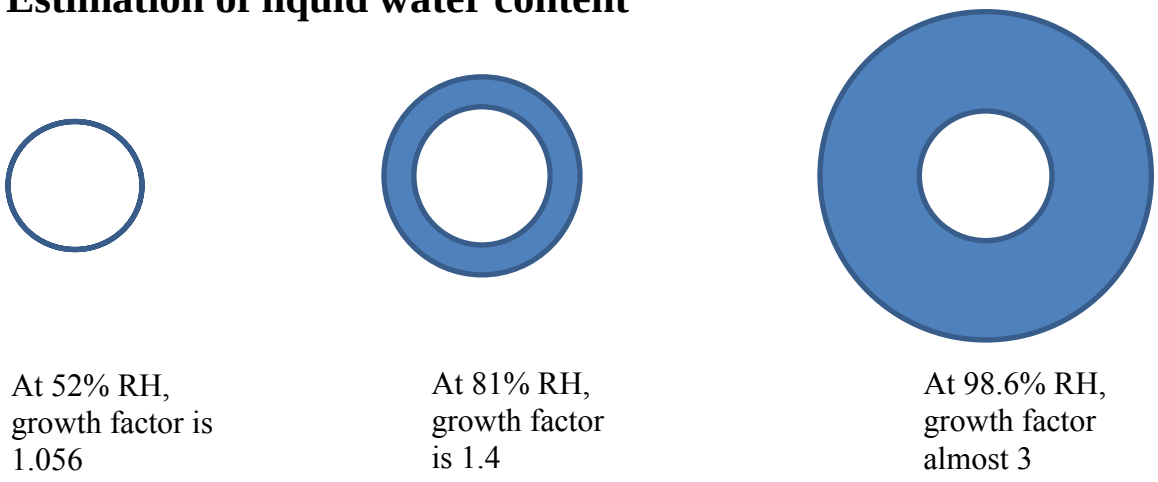

Figure 2.6: Activation of aerosol particles at different RH regimes. (Wex et al. 2008)

Study done by Wex et al. (2008) shows that activation of aerosol particles takes place at high RH regimes and hygroscopic growth of particles is observed. For estimation of water content we can use these particles and bin then on the basis of % RH. To have an estimate of total liquid water content in the winter fog at IISER Mohali for the months of December 2011, January 2012 and February 2012, we use $PM_{2.5}$ particles because PM_{10} particles are mainly dust, which is hydrophobic. This will provide a lower estimate of how much water is present in the region during fog period. We use hygroscopic growth factor to calculate the liquid water content. Provided is the formula,

$PM_{2.5}$ x (Hygroscopic growth factor)^3 – $PM_{2.5}$ = Total liquid water content ($\mu g/m^3$)

Where $PM_{2.5}$ values are in $\mu g/m^3$.

2.7 Estimation of S (VI) produced in the region

Using the selected emission ratio we predicted the SO_2 at source using the CO data collected at AAQS. SO_2 at source is already being measured at the receptor site. So we can estimate the total S (VI) produced by subtracting the measured SO_2 at receptor and the total S (IV) dissolved in the aqueous phase. We assume that everything is already in equilibrium by the time the air mass reaches the receptor site. By subtracting the dissolved S (IV), we removed the S (IV) that is present in the aqueous phase without being oxidized, so only the uptake and dissociation of S (IV) takes place in the aqueous phase.

Total S (VI) formation = SO_2 (predicted) – SO_2 (measured) – SO_2 (dissolved in aqueous phase)

Chapter 3

Results and discussions

3.1 SO_2 Trend

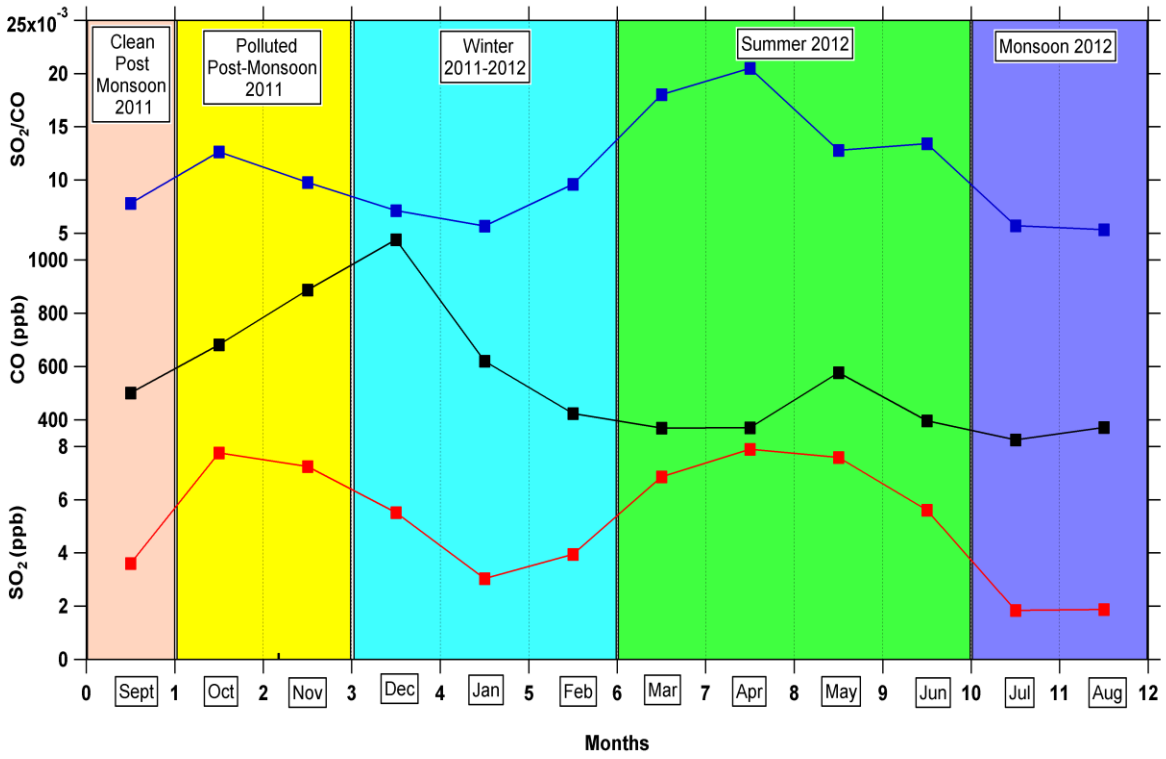

Figure 3.1: Monthly Averages for SO_2, CO and SO_2/CO ratio at IISER Mohali from September 2011 to August 2012.

From Figure 3.1, it is clearly observable that, monsoon is the cleanest season. Domestic combustion of biomass is limited to cooking and brick kilns do not operated due to flooding of the clay pits. Emission and production of SO_2 and CO is less than in other season and monsoon convection above the foothills of the Himalayas efficiently uplifts pollutants to higher altitudes so concentrations in the boundary layer are lower. However, given the fact

that anthropogenic sources with high emission ratios should dominate SO_2/CO ratios more than in any other season of the year, as their emission intensity does not vary significantly throughout the year (traffic, industries coal fired power plants) the low SO_2/CO can only be explained by wet scavenging of SO_2 and an increased conversion to sulfate in clouds Venkataraman et al. (1999). During clean post monsoon emissions pick up slightly (brick kilns resume operation) and the reduction in convective uplift leads to an additional increase in observed boundary layer mixing ratios. The decrease in wet scavenging and in the conversion rate to sulfate leads to an increase of the SO_2/CO ratios. Summer season shows low CO mixing ratios compared to post monsoon season, except during the month of May when crop residue burning is active. We expect similar emissions for summer and post monsoon season, therefore, the decrease in CO mixing ratio is probably due to a higher daytime boundary layer in summer. SO_2 mixing ratios in summer increase and the SO_2/CO ratio moves closer towards the expected emission ratio for a mix of biomass combustion, traffic and industrial sources, indicating SO_2 removal in summer is slow.

Polluted post monsoon is the season of crop residue burning. We have observed relatively high emission of CO during the month of November due to bio-mass burning and emission ratios close to but slightly higher than emission ratios expected for biomass combustion which can be explained by the fact that anthropogenic sources operate throughout the year. During winter season, in particular in December, high CO values were observed (due to additional combustion for domestic heating) but surprisingly very low SO_2 values which indicating a strong SO_2 sink. SO_2/CO ratios are lower than the ratios observed during crop residue burning and hence an increase in the fraction of biomass combustion is not a valid explanation for the decrease of the emission ratio. The winter season is characterized by frequent fog episodes, which could lead to an increase in the SO_2 to sulfate conversion. However, model calculations by Venkataraman et al. (1999), with a model that considered only clouds cover and not fog for calculating the aqueous phase sulfate production reported no increase in sulfate yields, coupled with a very long lifetime of sulfate during winter. We decided to look at SO_2 chemistry during the winter season, to investigate the importance of aqueous phase reactions in winter time fog for SO_2 removal.

3.2 Possible sinks for SO_2 at IISER Mohali

Since SO_2 average and median values are less during winter, there must various sinks responsible for SO_2 loss. As provided in the introduction, there are a lot of major sinks for SO_2 like oxidation by OH radicals Criegee intermediates, O3, H_2O_2, O_2 catalyzed by transition metal ions and wet deposition. For IISER Mohali, little to no rainfall was observed during the month of December 2011, January 2012 and February 2012 and the first rainfall was observed during the harvesting season i.e. month of March and April, so wet deposition cannot be the sink. Thus, it is either the photochemistry or the aqueous-phase oxidation/fog chemistry that is acting as a major sink of SO_2 for IISER Mohali during the winter season 2011-2012.

3.3 SO_2 Chemistry at IISER Mohali

To investigate whether photochemistry or the fog chemistry which is responsible for loss of SO_2 at our site we investigated diel profile of SO_2 and solar radiation as a function of relative humidity. Figure 3.2 shows the box and whisker plots of SO_2 and solar radiation for various Relative Humidity (RH) bins. The bottom and the top of the box are 25^{th} and 75^{th} percentile (the lower and upper quartiles respectively), the band near the middle of the box is 50^{th} percentile (the median) and the bottom and top whiskers show are the 10^{th} percentile and the 90^{th} percentile. Relative humidity bins are established based on the relative humidity observed at 12:00 noon (when the sun is at the highest point in the sky) and the full day is classified into a relative humidity bin based on the humidity observed during this time of the day. Bins are: < 30% RH , 30-40% RH, 40-50% RH, 50-60% RH, 60-70% RH, 70-80% RH, 80-90% RH and > 90% RH. In Figure 3.2, shows on left hand side the box and whisker plots for SO_2 in ppb and plots on the right hand side show box and whisker plots for solar radiation in W/m^2. Red line shows the median for every hour of the day.

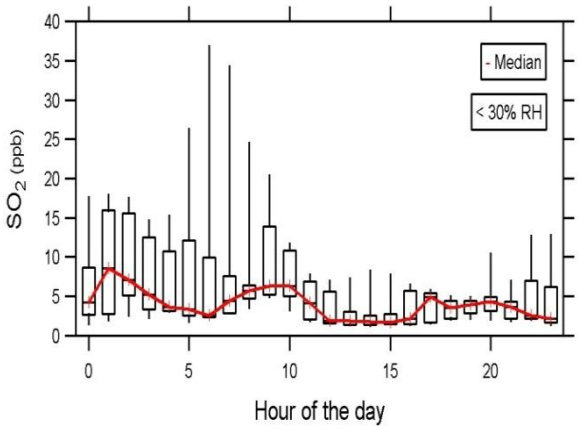
- Median
< 30% RH
SO2 (ppb)
Hour of the day

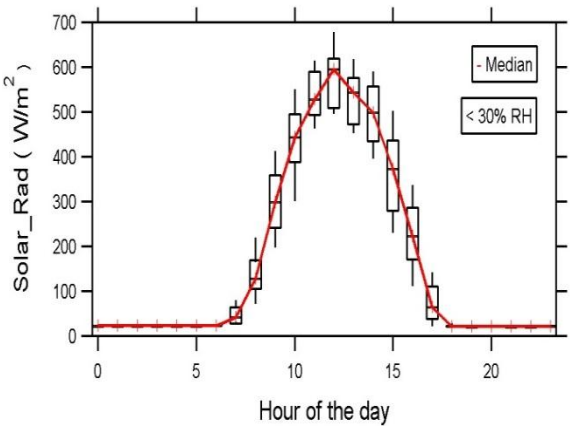
- Median
< 30% RH
Solar_Rad (W/m2)
Hour of the day

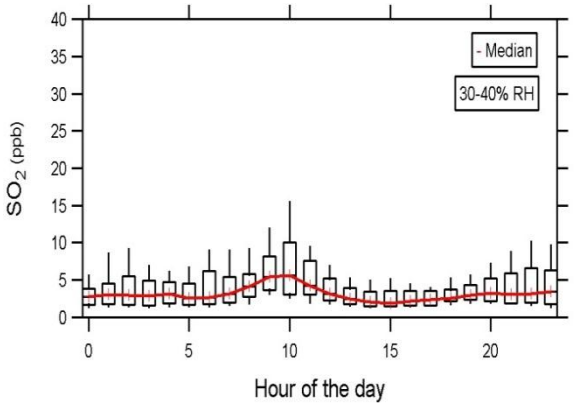
- Median
30-40% RH
SO2 (ppb)
Hour of the day

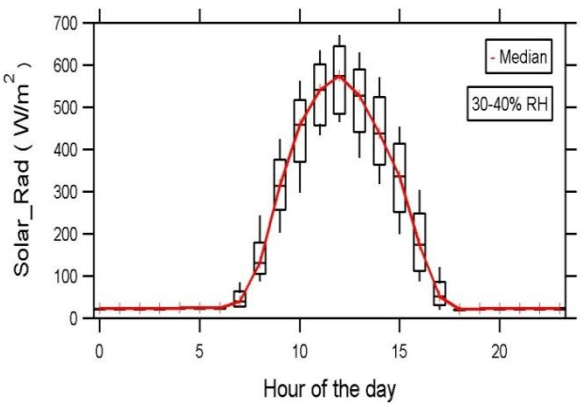
- Median
30-40% RH
Solar_Rad (W/m2)
Hour of the day

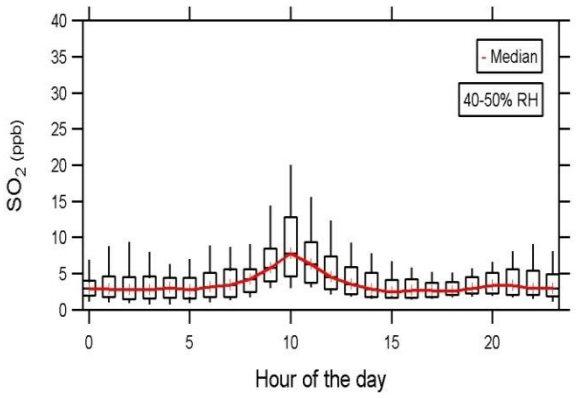
- Median
40-50% RH
SO2 (ppb)
Hour of the day

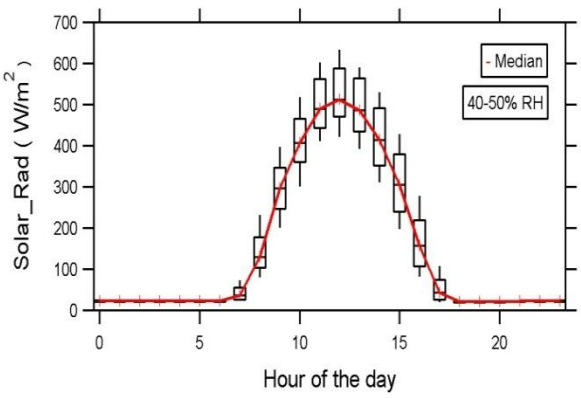
- Median
40-50% RH
Solar_Rad (W/m2)
Hour of the day

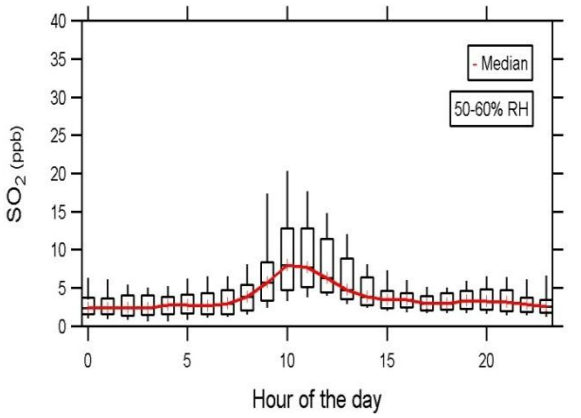
- Median
50-60% RH
SO2 (ppb)
Hour of the day

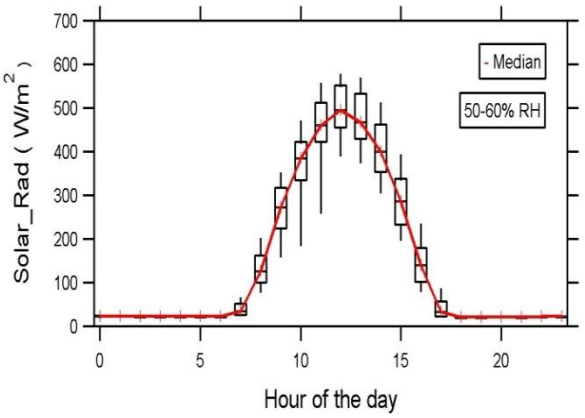
- Median
50-60% RH
Solar_Rad (W/m2)
Hour of the day

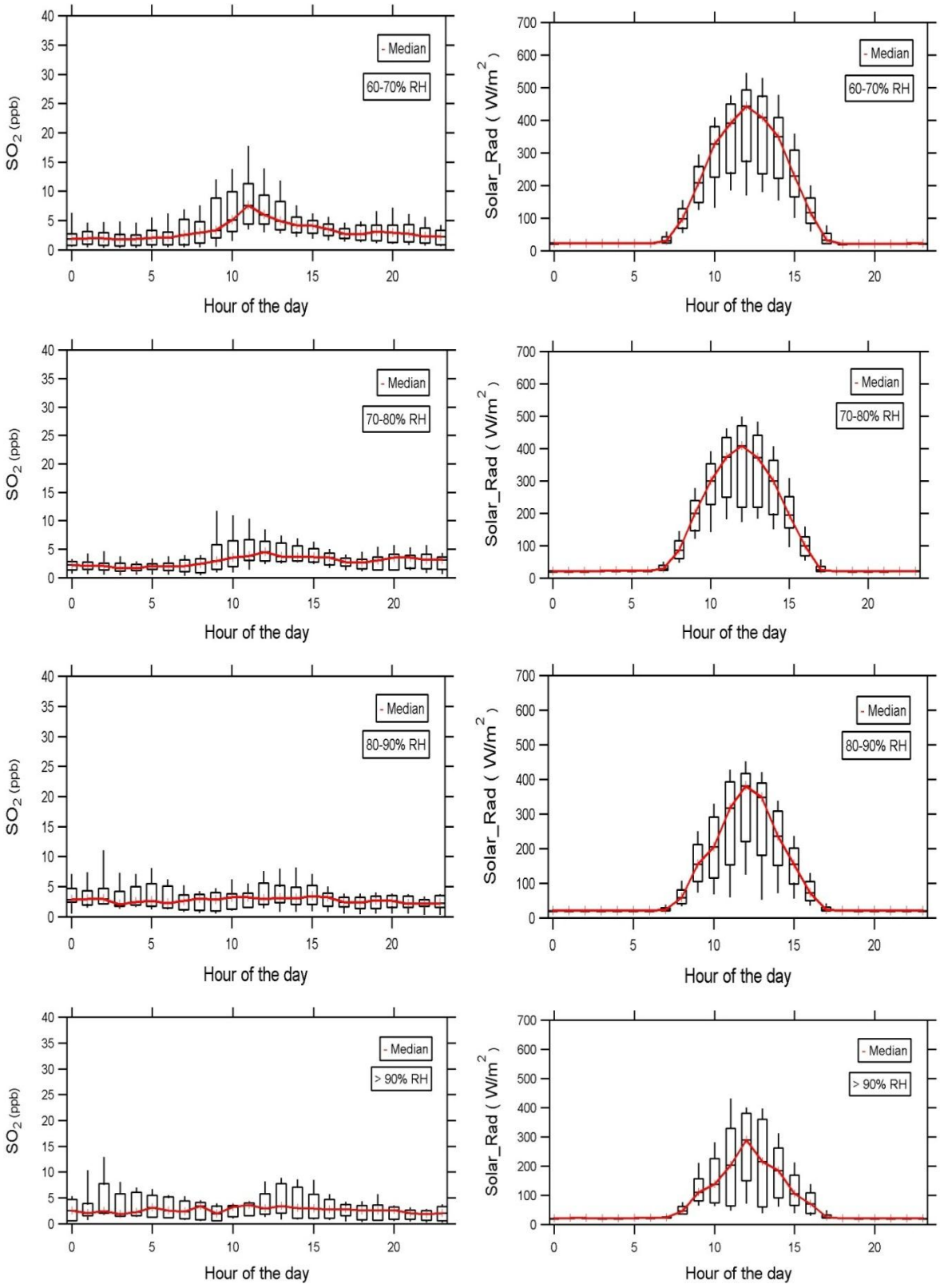

Figure 3.2: Median box and whisker plots for SO_2 and solar radiation for different Relative Humidity bins.

For days with low relative humidity we observe high daytime solar radiation. SO_2 mixing ratios at < 30% RH are high during the night, when the boundary layer is shallow and low during the day when the boundary layer is high and photochemistry is active, but statistics for this RH range is weak as few day during winter season had such low relative humidity. RH >30% are more frequent and SO_2 emissions follow a diel pattern with a peak around 10 in the morning. The height of the peak is least for the bin 30-40% RH and increases for increasing RH till the RH crosses a threshold of ~60% RH at the same time peak daytime radiation median deceases from 500-680 W/m² for 30-40% RH to 400-600 W/m² for 50-60% RH. Since solar radiation (surface warming) is closely coupled with boundary layer evolution the daytime boundary layer height would shrink with decreasing solar radiation. Once the relative humidity increases beyond 60% the daytime emission peak gradually disappears and solar radiation drops from 150-550 W/m² for 60-70% RH to 100-400 W/m² at > 90% RH. Since the daytime boundary layer would be continuously shrinking emissions should get concentrated within the boundary layer. The disappearance of the daytime SO_2 peak can hence only be explained by an increase in the SO_2 sink. We can conclude that due to the thickness of the fog, the photochemistry is suppressed when humidity is high and hence aqueous phase processes are the only plausible SO_2 sink.

3.4 Identification of Source

For the purpose of identifying a point source at our site, proper normalization is needed.

Firstly, distant sources can only be identified, when the SO2 loss rate is not too high. Therefore, we run our source receptor model only for values with a RH < 90%.
Secondly, some sources show a diel activity pattern that manifests itself in the diel box and whisker plots of SO_2. Therefore, we run our source receptor model separately for daytime and nighttime date.
Thirdly, the map should only contain pixels with a statistical significance. Therefore, the data is filtered such that the poisson statistical uncertainty for each pixel displayed in the map is <20%.

Using the Source-receptor model, residence time weighted average concentration plots were generated for SO_2 for different time scales and were overlaid on Google Earth to find out the exact location of the possible sources. 2 plots were run for 40-90% RH, one for day (7 am - 4 pm) and one for night time (7 pm - 5 am) for complete winter (10th December 2011 to 29th February 2012).

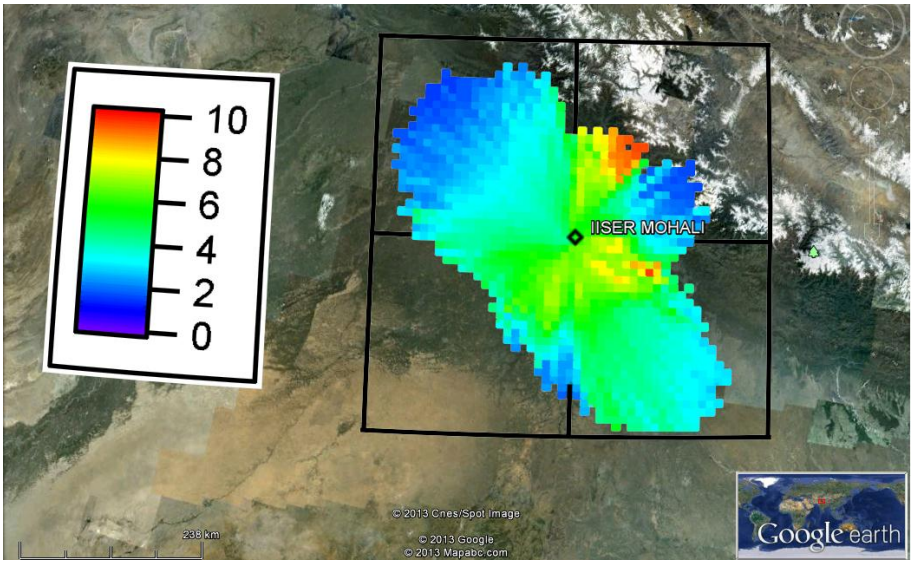

(a)

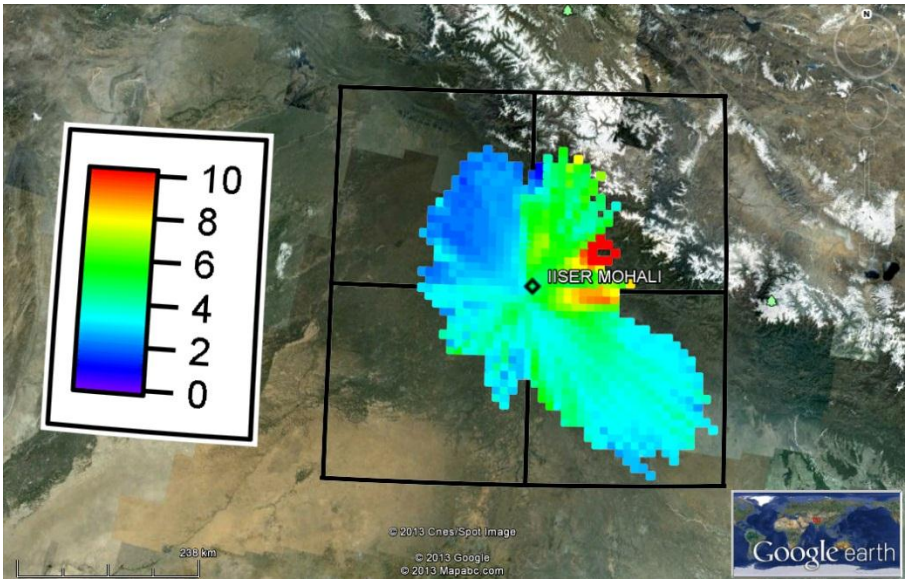

(b)

Figure 3.3: (a) and (b) Show the residence time weighted average concentration plots for SO_2 overlaid on Google Earth.

Figure 3.3 shows the regional sources of SO_2 for winter season. The color scale is set up to 10 ppb. As we move from blue to red, a grid becomes more and more probable of acting as a point source. We can see high concentration on the north-east direction of our location. However highest mixing ratios observed for the highest wind speeds are an indication of a source outside the model domain of (3 hours) possibly from long range transport. The exact location cannot be pinpointed with the help of this model. Whenever a pixel has been sampled with different residence times by a large enough number of data points the model can pinpoint the location of the sources. Towards the east of our site, yellow spots can be observed and they are not affected by long range transport so that might be a possible point source. We look at the day and night time plots as some sources are active during the day while some are active during the night. The model was again run for day time taking the values from 7 am to 4 pm. For the night time plot, the model was run from 7 pm till 5 am in the morning. Figure 3.3(a) and 3.3(b) show the day time and night time plots respectively. Both day and night time are also affected by long range transport. But there is one region in the day time plot when the source is active during the day only. And since that source is not affected by the long range transport, it can be concluded that it the point source and is the only major source which is suitable to investigate the SO_2 chemistry at our site.

Zooming in over that region on Google Earth, we observed that the region is KALA-AMB which actually is an industrial area in Sirmour District in the state of Himachal Pradesh and is located at distance of 50 km from the receptor site i.e. IISER Mohali

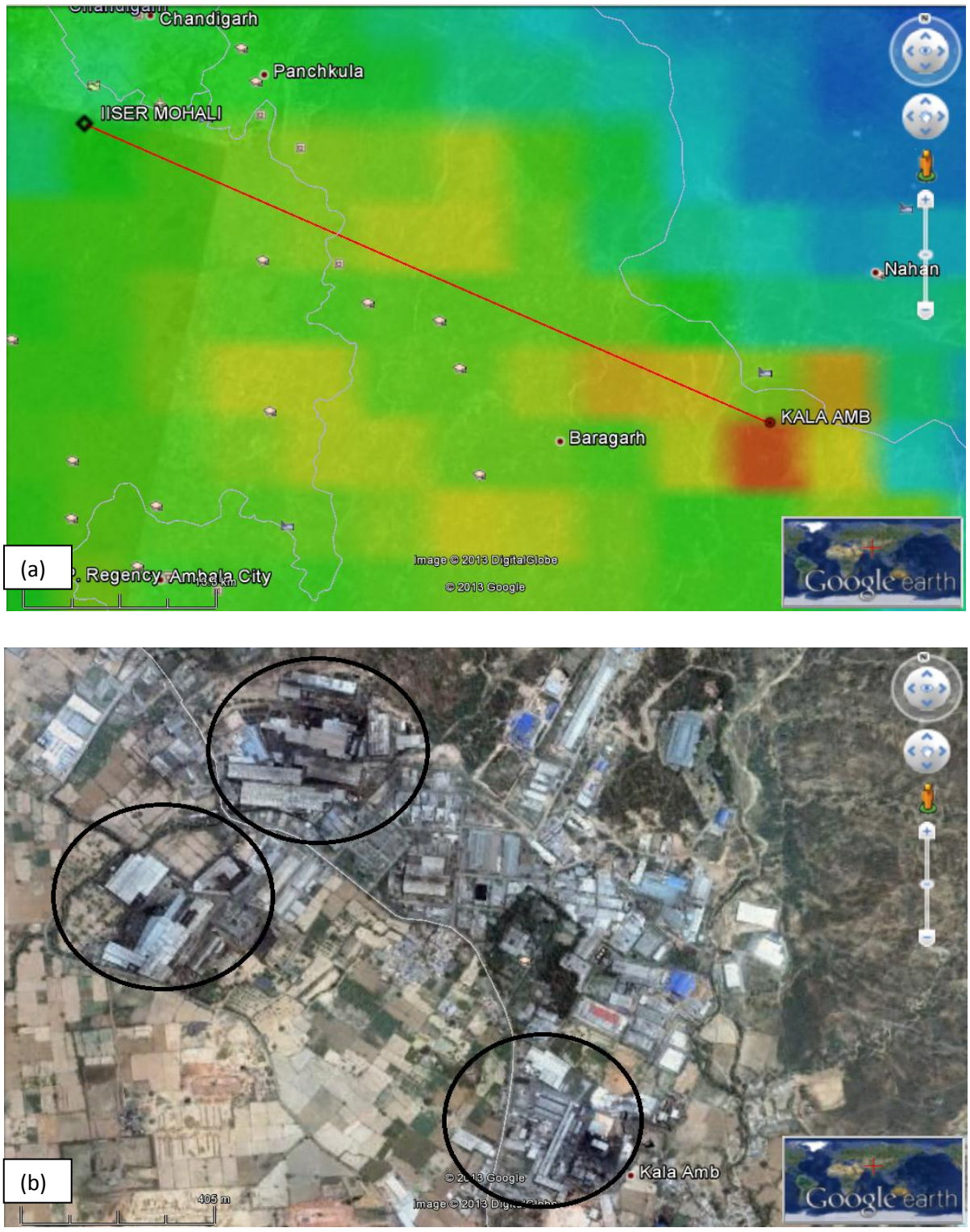

Figure 3.4(a) shows the direction of the major source, KALA-AMB from IISER Mohali with semi-transparent day-time plots from Google Earth. (b) shows the Zoom-in view of the industrial area in KALA-AMB.

KALA-AMB hosts production units for paper, metals, chemicals, thread mills and air conditioners. In Fig. 3.4 (b) coal stacks are clearly visible. As it is clear from Figure 3.3, KALA-AMB is active only during the day time, so the day time winter values were taken to calculate the loss rate of SO_2 emitted from this source.

3.5 Calculation of loss rate of SO_2

To calculate the loss rate of SO_2 emitted from KALA-AMB, wind-direction sector 99° - 115° was taken to make sure that the emission is not affected by any other near-by small scale emission. For the calculation of SO_2 loss, we need to measure the SO_2 at the receptor site and estimate SO_2 which should have reached our receptor site from that source. SO_2 data at source was taken from IISER-Mohali Ambient Air Quality Station (AAQS). However there was a need for estimation of how much SO_2 emitted from the source should have reached the receptor site.

SO_2 at source was calculated using the SO_2/CO emission ratio for industries (Table 2.5) since emissions at KALA-AMB come from an industrial source. Since CO has a life time of 1-2 months and concentration varies only due to dispersion and diffusion of the pollutants in the plume and doesn't change chemically, it was assumed that CO at source is of same concentration as we observe at our receptor site. Since Google Earth imagery indicates that the sources of our emissions are industries and the black areas outside some of the complexes indicate handling/storage of coal we used the emission ratio of industrial coal for our calculations.

Emission ratio was taken as 490/4088 using the data from Ohara et al. 2007. Since emission ratio was known and CO values were obtained from IISER-Mohali AAQS, the SO_2 mixing ratio of SO2 that should have been observed at the receptor site was calculated using emission ratio. Data for the sector 99° - 115° was then separated on the basis of different RH regimes and first order kinetics was applied to obtain the loss rate (per second).

$$\ln SO_2/SO_{2_0} = -k.t$$

Where, SO_2 = SO_2 at receptor site and SO_{20} = SO_2 at source, k = rate coefficient and t = time (in seconds)

Since the species in emission ratio were measured in unit of mass and the measurements of SO_2 and CO at IISER Mohali are done in unit of concentration, conversion was using the formula and loss rates were calculated.

Table 3.1: Loss rate of SO_2 for different RH regimes as a function of transport time (in seconds)

Actual fitted line					**Forcing the fitted line to pass through zero**	
% RH regime	**Loss rate of SO_2 (per s)**	**Uncertainty**	**Intercept**	**Uncertainty**	**New Loss rate (per s)**	**Corresponding Uncertainty**
40-50	4.2×10^{-5}	$\pm 0.8 \times 10^{-5}$	-0.3	± 0.2	5.2×10^{-5}	$\pm 0.3 \times 10^{-5}$
50-60	5.9×10^{-5}	$\pm 1.1 \times 10^{-5}$	0.0	± 0.3	6.0×10^{-5}	$\pm 0.3 \times 10^{-5}$
60-70	3.8×10^{-5}	$\pm 1.7 \times 10^{-5}$	-0.9	± 0.4	7.0×10^{-5}	$\pm 0.8 \times 10^{-5}$
70-80	2.5×10^{-5}	$\pm 0.7 \times 10^{-5}$	-1.4	± 0.2	8.4×10^{-5}	$\pm 1.4 \times 10^{-5}$
80-90	7.7×10^{-5}	$\pm 2.5 \times 10^{-5}$	0.0	± 0.6	7.58×10^{-5}	$\pm 0.8 \times 10^{-5}$

Calculating an estimate of loss rate at > 90% RH provides information that the loss rate is more than 2.19×10^{-4} per seconds for more than 90% RH. Intercept provides the information about the emission inventory for SO_2. It can be observed that the loss rate increases as we go to higher RH regimes with exceptions at 60-70% RH and 70-80% RH regimes which is possible because of the interference with other near-by source/sources which is/are not active though-out the season but is/are interfering with SO_2 plume coming out from the industries in KALA-AMB. All the other humidity regimes except these 2 show that the most prominent source for SO_2 in the region is KALA-AMB and the line fit passes through zero, indicating that the emission ratio selected for industries i.e. 490/4088 matches with the emission ratio for the industries which are present in KALA-AMB. However we do not have control over the sources so we forced all the lines to pass through zero and that's how we got the new loss

rates with new uncertainties. It can be observed that since all the humidity regimes except 70-80% RH do not have high uncertainty because the emission ratio that we selected matched the emission ratio of the industries in KALA-AMB giving near-zero intercepts except one humidity regimes i.e. 70-80% RH.

As water is ubiquitous in the atmosphere, it interacts with the aerosol particles, hydrates the particles and leads to the formation of cloud droplets with increase in size. This is called the hygroscopic growth of aerosol particles. Various studies have been done on hygroscopic growth of aerosols particles. A study on hydroscopic growth done by Wex et al. (2008) provides a data that as RH increases, there is an increase in growth factor. At 52% RH, growth factor is 1.056, at 81% RH, growth factor is 1.4 and at 98.6% RH, growth factor is almost 3. So at 99% RH, particle is almost 3 times of its regular size. Here is an estimate of liquid water content in the fog during the winter season at IISER Mohali.

Table 3.2: Using the data provided by Wex et al. (2008), here is an estimate of total liquid water content in the winter fog at IISER Mohali at various RH regimes.

% RH Regime	**Total water content (µg/m^3)**
50-60	55.21
60-70	171.43
70-80	301.32
80-90	406.19
>90	5936.81 – 19 (HG 3-1000)

$PM_{2.5}$ values were taken from the Ambient Air Quality Station Data at IISER Mohali. So the water content in the region varied from value as low as 55.21 x 10^{-6} g/m^3 at 50-60% RH to 5.93 x 10^{-3} g/m^3 at >90% RH. Still it is quite less compared to the water content present in clouds, which is 0.1 – 0.3 g/m^3 (Seinfeld and Pandis, 1998). The upper limit for the liquid water content for the bin 90-100% RH has been estimated assuming a hygroscopic growth factor of 1000 for all PM2.5 particulate to provide and extreme upper limit for the possible liquid water content.

From loss rates it is clearly observable that loss of SO_2 is higher for high RH regimes. The actual liquid water content is a very crucial parameter, as the speed of oxidation in aqueous phase depends mainly on liquid water content and the availability of oxidants in the atmosphere (Pandis and Seinfeld, 1989). In clouds because of sufficiently high liquid water content, the oxidation is in aqueous phase and significantly faster (Chameides and David, 1982).Oxidation of SO_2 is very less in aerosols when compared to clouds (Liang and Jacobson, 1999). The peak daytime radiation can serve as a measure of the actual extent of fog for all RH bins. If the peak daytime radiation decreases, this can only be explained through an extreme increase in aerosol dry mass or by factoring in hygroscopic growth of particles under ambient conditions. Therefore, we use the measured change in light extinction as a function of relative humidity and Mie theory as a second estimate of how much liquid water is really present in the aerosol phase.

3.6 Estimation of S (VI) produced in the region

Using the method provided in material and methods section we have estimated the S (VI) production after the air mass has moved for 6 hours starting from the source location. Data is then binned for various RH regimes to get an estimated of how much sulfate is formed at different RH.

Table 3.3: Table showing the Total S (VI) produced as the percentage of initial SO_2 at the source

Liquid Water Content (LWC) g/m^3	**Total S(VI) (as % of initial SO_2)**
- (40-50 % RH)	~ 66
0.55 x 10^{-3} (50-60% RH)	~ 75
1.71 x 10^{-3} (60-70% RH)	~ 85
3.01 x 10^{-3} (70-80%RH)	~ 87
4.06 x 10^{-3} (80-90% RH)	~ 87
59.36 x 10^{-3} – 19.78 (> 90% RH)	~ 96

Studies provide information that below 50% RH there is no liquid water content in particles and hence there is no hygroscopic growth. However, we observe a total S (VI) production of ~ 66% of the initial SO_2 present.

A study of SO_2 oxidation pathways over a range of liquid water contents done by Liang and Jacobson (1999) shows that the reactions currently included into atmospheric chemistry models can only account for a SO_2 to sulfate conversion of < 20% of the initial SO_2 in 6 hours, unless the water content in the aerosol phase is significantly higher than the water content estimated using conventional hygroscopic growth factors. Currently, global models do not consider aqueous phase chemistry reaction at <100% RH except for reactions that take place on sea salt aerosol above the ocean. Below is a table that has been modified from the

information provided by Liang and Jacobson (1999) showing the total sulfate production after 6 hours of the reaction starting time.

Table 3.4: Total S (VI) production by various oxidants at different Liquid Water Content (LWC) regime.

LWC g/m^3	**OH (aq) % of initial SO_2**	**OH (g) % of initial SO_2**	**H_2O_2 (aq) % of initial SO_2**	**O_3 % of initial SO_2**	**Total % of initial SO_2**
3×10^{-4}	-	20	-	-	20
0.3	5	15	50	-	70
3	40	< 5	40	< 5	90

According to this study, at low water content such as 3×10^{-4} g/m^3 only the gas phase oxidation by OH radicals is responsible for sulfate production and leads to the sulfate formation of ~ 20% of initial SO2 taken. Even if we look at the upper limit of water content such as 0.3 g/m^3, we observe ~ 70% conversion of initial SO_2 to sulfate. Even after considering the high liquid water content of 0.3 g/m^3, the present models cannot explain ~ 87% conversion of the initial SO2 present to sulfate that we observe at our site for water content as low as 4.06×10^{-3} g/m^3.

The scheme produces rapid SO_2 loss / SO_4 only while assuming very high liquid water content. Such high liquid water content in the aerosol phase is unlikely for 47% RH, therefore, alternate explanations for the observed loss rate are required.

3.7 Conclusion

We find that the SO_2 loss rate at our site cannot be explained using H_2O_2, O_3 and OH chemistry and the gas phase chemistry currently incorporated into the models. The loss rate is a function of relative humidity (our best proxy for fog liquid water content) indicating that part of the missing oxidation occurs in the aqueous phase. Possibly due to TMI catalyzed oxidation, as the source of plume includes metal industries.

Even under conditions where global models do not consider aqueous phase chemistry to occur we observe high conversion rates. Criegee intermediates need to be incorporated into the gas phase chemistry to see if they close part of the gap. The contribution of in-cloud oxidation pathway to sulfate formation ranges from 75% (models only including H_2O_2) to 83% (Models including H_2O_2, O_3 and TMI's) between different global climate models that contributed to the fourth IPCC Report. This uncertainty contributes to the uncertainty regarding the magnitude of global aerosol cooling (-1.8 W m^{-2} and -0.3 W m^{-2}.). None of the models currently includes the recently discovered second source of H_2SO_4 (g) (Boy et al., 2013) and few include TMI. So there is a need to include the newly discovered oxidation pathways and the fact that substantial amounts of water can be found in the aerosol phase even at relative humidities well below 100% in models to have a better estimate of sulfate production and hence better estimate of global cooling due to aerosols. Moreover, in the Indo-Gangetic Plain, where pH < 6 is rarely observed in rain and fogwater and the pH is usually found to be close to 7 aerosol chemistry may need to be incorporated into the model to account for buffering of pH e.g. by $CaCO_3$ through the reaction $CaCO_3 + H_2SO_4 \rightarrow$ gypsum + HCO_3^- + H^+ or NH_4^+.

Such buffering alone could lead to substantially increased S (VI) production rates, compared to the Jacobson (1999) study, as the aerosol pH in their model drops from 7 to 4.5 for 3 g/m³ liquid water content and to 2.6 for 0.3 g/m³ liquid water content. The rapid drop in droplet pH is one of the reasons for self-quenching of reactions that occur only at pH>6 and has led to conclusion that such reactions can safely be neglected in global model. However, incorporating aerosol chemistry into the model may change this view at least on a regional scale.

BIBLIOGRAPHY

Alexander, R. J. Park, D. J. Jacob, Q. B. Li, and R. M. Yantosca, Sulfate formation in sea-salt aerosols: Constraints from oxygen isotopes, J. Geophys. Res., 110, D10307, 2005.

Andreae M. O. and P. Merlet, Emission of trace gases and aerosols from biomass burning, Global Biogeochemical cycles, 15(4), 955-966, 2001.

Atkinson R., D. L. Baulch, R. A. Cox, J. N. Crowley, R. F. Hampson, R. G. Hynes, M. E. Jenkin, M. J. Rossi, and J. Troe, Evaluated kinetic and photochemical data for atmospheric chemistry: Volume I – gas phase reactions of Ox, HOx, NOx and SOx species, Atmos. Chem. Phys., 4, 1461–1738, 2004.

Atmospheric Chemistry and Physics, Seinfeld and Pandis, Wiley and Sons, 1998.

Benson, D. R., Young, L. H., Kameel, F. R., and Lee, S. H.: Laboratory-measured nucleation rates of sulfuric acid and water binary homogeneous nucleation from the SO_2 + OH reaction, Geophys. Res. Lett., 35, L11801, 2008.

Bengtsson, S., and I. Bjerle, Catalytic-Oxidation of Sulfite in Diluted Aqueous-Solutions, Chemical Engineering Science, 30(11), 1429-1435, 1975

Berndt, T., Stratmann, F., Brasel, S., Heintzenberg, J., Laaksonen, A., and Kulmala, M.: SO_2 oxidation products other than H_2SO_4 as a trigger of new particle formation. Part 1: Laboratory investigations, Atmos. Chem. Phys., 8, 6365-6374, 2008.

Berresheim, H., Elste, T., Tremmel, H. G., Allen, A. G., Hansson, H. C., Rosman, K., Dal Maso, M., Makela, J. M., Kulmala, M., and O'Dowd, C. D.: Gas-aerosol relationships of H2SO4, MSA, and OH: Observations in the coastal marine boundary layer at Mace Head, Ireland, J. Geophys. Res.-Atmos.,107, 2002.

Boy, M., Mogensen, D., Smolander, S., Zhou, L., Nieminen, T., Paasonen, P., Plass-Dülmer, C., Sipilä, M., Petäjä, T., Mauldin, L., Berresheim, H., and Kulmala, M.: Oxidation of SO_2 by stabilized Criegee Intermediate (sCI) radicals as a crucial source for atmospheric sulphuric acid concentrations, Atmos. Chem. Phys. Discuss., 13, 3865-3879, 2013.

Brandt C. and L. Elding, ROLE OF CHROMIUM AND VANADIUM IN 'THE ATMOSPHERIC OXIDATION OF SULFUR (IV). Atmos. Envron., 32(4), pp. 797-800, 1998.

Brandt C. and Rudi van Eldik, Transition Metal-Catalyzed Oxidation of Sulfur(lV) Oxides. Atmospheric-Relevant Processes and Mechanisms, Chem. Rev., 95, 119-190, 1995.

Chameides, W.L., and D.D. Davis, The free-radical chemistry of cloud droplets and its impact upon the composition of rain, J. Geophys. Res., 87, 4863-4877, 1982.

Chemistry: The Molecular Science Moore, J., Stanitski, C., and Jurs, P., Brooks/Cole - Thomson Learning, USA, 2005.

Crutzen, P.J., The possible importance of CSO for the sulfate aerosol layer of the stratosphere, Geophys. Res. Lett., 3, 73-76, 1976.

Dentener, F., J. Williams, and S. Metzger, Aqueous phase reaction of HNO_4: The impact on tropospheric chemistry, J. Atm. Chem., 41, 109-134, 2002.

Eriksen, T. E.: Sulfur Isotope Effects 1. Isotopic Exchange Coeffcient for Sulfur Isotopes ^{34}S-^{32}S in System SO_2 (g)-HSO_3(aq) at 25, 35, and 45°C, Acta Chemica Scandinavica, 26, 573-580, 1972.

Feingold, G., G. J. Frost, and A. R. Ravishankara, Role of NO_3 in sulfate production in wintertime northern latitudes, J. Geophys. Res., 107(D22), 4640, 2002.

Garg S., V. Sinha and B. Sinha, Taking potential probability function maps to the local scale and matching them with land use maps. Geophysical Research Abstracts Vol. 15, EGU2013-401-4, 2013.

Graedel, T.E., and C. J. Weschler, Chemistry within aqueous atmospheric aerosols and raindrops, Rev. Geophys., 19, 505-539, 1981.

Grgic I., V. Hudnik, M. Bizjak, J. Levec, Atmos. Environ., 25, 1991.

Hoppel,W., Frick, G., Fitzgerald, J., and Wattle, B.: A cloud chamber study of the effect that non precipitating clouds have on the aerosol size distribution, Aerosol Science and Technology, 20, 1 -30, 1994.

Junge, C.E., C.W. Chagnon, and J.E. Manson, Stratospheric Aerosols, J. Meteorology, 81-108, 1961.

Kotronarou, A., and L. Sigg, SO_2 Oxidation in Atmospheric Water - Role of Fe (II) and Effect of Ligands, Environ. Sci. Technol., 27(13), 2725-2735, 1993.

Kulmala, M.: How particles nucleate and grow, Science, 302, 1000-1001, 2003.

Kulmala, M., Vehkamaki, H., Petaja, T., Maso, M. D., Lauri, A., Kerminen, V. M., Birmili, W., and McMurry, P. H.: Formation and growth rates of ultrafine atmospheric particles: a review of observations, Journal of Aerosol Science, 35, 143-176, 2004.

Laaksonen, A., Kulmala, M., Berndt, T., Stratmann, F., Mikkonen, S., Ruuskanen, A., Lehtinen, K. E. J., Maso, M. D., Aalto, P., Petaja, T., Riipinen, I., Sihto, S. L., Janson, R., Arnold, F., Hanke, M., Ucker, J., Umann, B., Sellegri, K., O'Dowd, C. D., and Viisanen, Y.: SO_2 oxidation products other than H_2SO_4 as a trigger of new particle formation. Part 2: Comparison of ambient and laboratory measurements, and atmospheric implications, Atmos. Chem. Phys., 8, 7255-7264, 2008.

Liang J. and M. Z. Jacobson, A study if sulfur dioxide oxidation pathways over a range of liquid water contents, pH values and temperatures, J. Geophys. Res., 104, 13,749-13,769, 1999.

Lyons J. R., Chapter 5 Photolysis of Long-Lived Predissociative Molecules as a Source of Mass-Independent Isotope Fractionation: The Example of SO2, In: Michael E. Goodsite and Matthew S. Johnson, Editor(s), Advances in Quantum Chemistry, Academic Press, 55, 57-74, 2008.

Martin, L.R., and M. W. Hill, The iron catalyzed oxidation of sulfur: reconciliation of the literature rates, Atmos. Env., 25A, 1487-1490, 1987.

Model 43i Trace Level-Enhanced Instruction Manual, Pulsed Fluorescence SO2 Analyzer Part Number 102780-00, 14 Jan 2008.

Ohara, T., Akimoto, H., Kurokawa, J., Horii, N., Yamaji, K., Yan, X., and Hayasaka, T.: An Asian emission inventory of anthropogenic emission sources for the period 1980–2020, Atmos. Chem. Phys., 7, 4419-4444, 2007.

Okabe H., Fluorescence and predissociation of sulfur dioxide, J. Amer. Chem. Soc., 93, 7095, 1971.

Omenetto, N. and G. D. Boutilier Pulsed vs. continuous wave atomic fluorescence spectrometry, Analytical Chemistry, 49(7): 1076-1078, 1977.

Pandis, S.N., and J.H. Seinfeld, Sensitivity analysis of a chemical mechanism for aqueous-phase atmospheric chemistry, J. Geophys. Res., 94, 1105-1126, 1989.

Pierce J. R., M. J. Evans, C. E. Scott, S. D. D'Andrea, D. K. Farmer, E. Swietlicki, and D. V. Spracklen5: Weak global sensitivity of cloud condensation nuclei and the aerosol indirect effect to Criegee+SO_2 chemistry Atmos. Chem. Phys., 13, 3163 -3176, 2013.

Pöhlker, C., Wiedemann, K., Sinha, B., Shiraiwa, M., Gunthe, S. S., Smith M., Hang, S., Artaxo, P., Chen, Q., Cheng, Y., Elbert, W., Gilles, M.K., Kilcoyne, A. L. D., Moffet, R., Weigand, M., Martin, S. T., C., Pöschl, U., and Andreae, M. O.: STXM-NEXAFS Investigations of Laboratory Secondary Organic Aerosols and Amazonian Background Aerosols. Science, 337, 1075-1078, 2012.

Pueschel, R.F., Stratospheric aerosols: formation, properties, effects, J. Aerosol. Sci., 27, 383-402, 1995.

Solomon, S., Qin, D., Manning, M., Chen, Z., Marquis, M., Averyt, K., Tignor, M., and H.L., M.: Climate Change 2007: The physical science basis. Contribution of the working group I to the Fourth Assessment Report of the Intergovernmental Panel on Climate Change., p. 996, Cambridge University Press, New York, 2007.

Tursic, J., Grgic, I., Podkrajsek, and B., Influence of ionic strength on aqueous oxidation of SO2 catalyzed by manganese, Atmos. Environ., 37(19), 2589-2595, 2003.

Venkataraman C., C. Bharadwaj, A. Patwardhan, Anthropogenic sulphate aerosol from India: estimates of burden and direct radiative forcing, Atmos. Environ., 33, 3225-3235, 1999.

Venkataraman C., G. Habib, D. Kadamba, M. Shrivastava, J.F. Leon, B. Crouzille, O. Boucher, and D. G. Streets, Emissions from open biomass burning in India: Integrating the inventory approach with high-resolution Moderate Resolution Imaging Spectroradiometer (MODIS) active-fire and land cover data, Global Biogeochem. Cycles, 20, GB2013, 2006.

Wex H., F Stratmann, T Hennig, S Hartmann, D Niedermeier, E Nilsson, R Ocskay, D Rose, I Salma and M Ziese, Connecting hygroscopic growth at high humidities to cloud activation for different particle types, Environ. Res. Lett., 3, 2008.

Worden, H. M., Y. Cheng, G. G. Pfister, G. R. Carmichael, Q. Zhang, D. G. Streets, M. N. Deeter, D. P. Edwards, J. C. Gille, and J. R. Worden, Satellite-based estimates of reduced CO and CO2 emissions due to traffic restrictions during the 2008 Beijing Olympics, Geophys. Res. Lett., 39, L14802, 2012.

Zhenjiang He; Guanling Yang; Jianwen Xiong; Zuohua Huang; Hongzhong Chen; Yongzhi Lai, Design on Monitor system of Sulfur Dioxide Concentration by UV Fluorescence Method Dept. of Physics, South China Normal University, Guangzhou, 510631, China, SPIE Vol. 4927, 830-833, 2002.

Zuo, Y. G., and J. Zhan, Effects of oxalate on Fe-catalyzed photo-oxidation of dissolved sulfur dioxide in atmospheric water, Atmos. Environ., 39(1), 27-37, 2005.